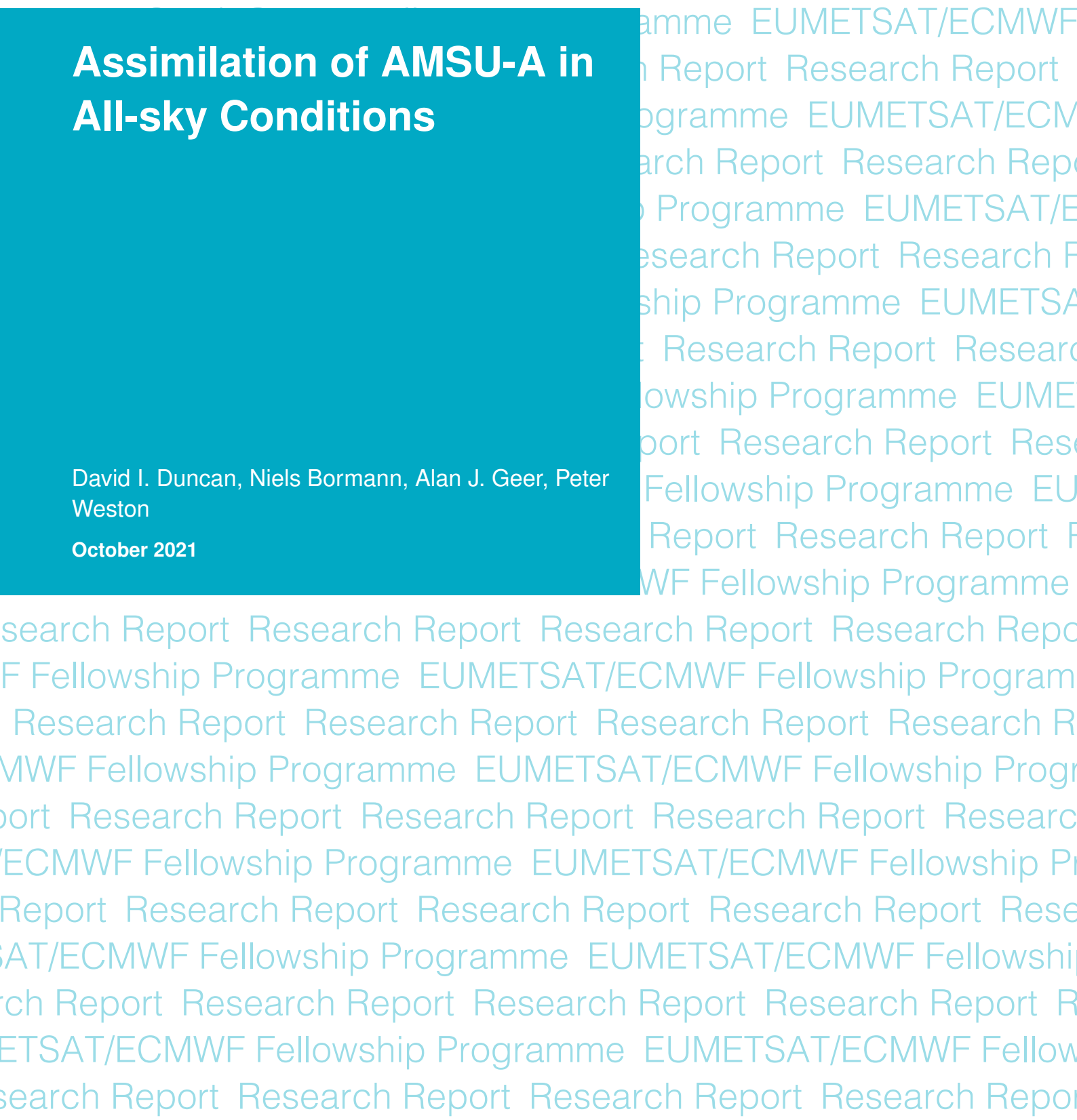# EUMETSAT/ECMWF Fellowship Programme Research Report

57

Assimilation of AMSU-A in All-sky Conditions

David I. Duncan, Niels Bormann, Alan J. Geer, Peter Weston

October 2021

Abstract

Radiances from microwave temperature sounders have been assimilated operationally at ECMWF for two decades, but observations significantly affected by clouds and precipitation have been screened out. Extending successful assimilation beyond clear-sky scenes is a challenge that has taken several years of development to achieve. In this paper we describe the all-sky treatment of AMSU-A, which enables greater numbers of temperature sounding radiances to be used in meteorologically active parts of the troposphere. Successful all-sky assimilation required combining lessons learnt from the clear-sky assimilation of AMSU-A with the approach initially developed for humidity-sensitive microwave radiances. This concerned particularly observation thinning, error modelling, and variational quality control.

As a result of the move to all-sky assimilation, the forecast impact of AMSU-A now replicates and exceeds that of the previous clear-sky usage. This is shown via trials in comparison to the current ECMWF assimilation system, judged with respect to forecast scores and background fits to independent observations. Persistently cloudy regions and phenomena such as tropical cyclones are better sampled when assimilating AMSU-A in all-sky conditions, causing an increase of about 13% in used channel 5 radiances globally. These impacts are explored, with an emphasis on tropical cyclones in the 2019 season. Independent observations provide consistent evidence that representation of humidity is improved, for example, while extratropical Z500 forecasts are improved by about 0.5% out to at least day 2. On the strength of these results, assimilation of AMSU-A moves to all-sky conditions with the upgrade to IFS cycle 47R3 in October 2021.

1 Introduction

1.1 Background

The Advanced Microwave Sounding Unit-A (AMSU-A) is one of a suite of sensors providing accurate atmospheric profiling capability from the near-surface to the upper stratosphere. After some previous success in directly assimilating microwave temperature sounder radiances (Andersson *et al.*, 1994), AMSU-A quickly became a valuable asset for improving numerical weather prediction (NWP) forecasting capabilities (English *et al.*, 2000). Nine satellites have held AMSU-A sensors, starting with NOAA-15 in 1998 (see Table 1). As of 2021 there are seven functioning AMSU-A sensors in orbit, on board satellites spanning two decades of launches.

Microwave temperature sounding has been and remains a key component of the global observing system for driving NWP forecast skill (e.g. Cardinali, 2009; Geer *et al.*, 2017; Bormann *et al.*, 2019). The main advantage of microwave temperature sounding, and a key reason for the success of AMSU-A in NWP, is its relative insensitivity to clouds, with tropospheric channels primarily sensitive to air temperature alone. Thus microwave sounding channels hold useful, unique information on the atmospheric state beneath cloud tops. In addition to this advantage based in atmospheric physics, the impact of AMSU-A in NWP is partially attributable to a strength in numbers (Duncan *et al.*, In press) and the excellent global coverage afforded by its cross-track swath width of over 2000 km.

At the European Centre for Medium-Range Weather Forecasts (ECMWF), AMSU-A channels 5 to 14 are actively assimilated. These are channels with primary sensitivity to temperature from the mid-troposphere through upper stratosphere (see Table 2), constituting all sounding channels of the instrument with exception of channel 4, which mixes lower tropospheric sounding with surface sensitivity. Channels 1-3 and 15 are considered window or "imager" channels as their main sensitivity is to the surface and

Table 1: Satellites holding AMSU-A sensors. End of life (EOL) is given for the sensor, not the satellite. Broken channels indicate those declared failed by the data provider or with high noise that precludes their active use (as of mid 2021).

Satellite	Launch	EOL	Broken Channels
NOAA-15	1998	-	6, 11, 14
NOAA-16	2000	2014	4, 8, 9
NOAA-17	2002	2003	N/A
Aqua	2002	-	1, 2, 4, 5, 6, 7, 14
NOAA-18	2005	-	9
Metop-A	2006	2021	7, 8
NOAA-19	2009	-	7, 8
Metop-B	2012	-	15
Metop-C	2018	-	-

hydrometeors rather than temperature profile information; these are used to gather surface emissivity and cloud information to aid the assimilation of sounder channels but are not themselves assimilated. Channels 5-14 have been assimilated in clear-sky conditions at ECMWF for over twenty years.

Assimilation in the "clear-sky" paradigm includes no hydrometeors in the radiative transfer, ignoring potential scattering or emission signals from clouds or precipitation. This is simpler and computationally cheaper, with increments going primarily to air temperature. Frequencies near 55 GHz mostly pass through cirrus clouds that can strongly attenuate shorter wavelength radiation. It is only in the presence of optically thick clouds and precipitation that a significant effect is evident in the brightness temperatures (TBs). Even then, this is only a concern for the lowest-peaking channels on AMSU-A (5-7), as clear-sky radiative transfer is always sufficient for stratospheric channels. Observations significantly affected by hydrometeors are avoided using screening procedures. These utilise the imager channels to detect thicker liquid clouds and scattering from precipitation that violate the clear-sky assumption and risk erroneous increments. In addition to screening, at the prior stage of data thinning, observations are selected based on the likelihood of being cloud-free. This causes inherently biased sampling but permits more data to go through the clear-sky framework.

"All-sky" assimilation is an approach for treating satellite radiances in all atmospheric conditions, from clear skies to precipitation. A situation-dependent observation error model retains similar error specifications in clear conditions whilst assigning larger errors in cloudy conditions. At ECMWF, all-sky assimilation was first pioneered using radiances from microwave imagers and then microwave humidity sounders (Bauer *et al.*, 2010; Geer and Bauer, 2010; Geer *et al.*, 2014). This has gradually led to microwave observations that are sensitive to humidity, clouds, and precipitation becoming as important to short-range forecast impact as the clear-sky temperature-sounding microwave observations (Geer *et al.*, 2017). There has been a gradual proliferation of NWP centres around the world utilising all-sky assimilation (Geer *et al.*, 2018).

1.2 Temperature Sounding in All-sky Conditions

If channels 5 and above on AMSU-A are seldom affected by significant enough clouds or precipitation to violate the clear-sky assumption, why bother with all-sky assimilation for these channels? Can much be

Table 2: Channels on AMSU-A are given by number, centre frequency in GHz, and peak of the weighting function in pressure. Channels' peak sensitivity is given as the approximate pressure maxima range of the weighting function from nadir to scan edge.

	Frequency [GHz]	Peak sensitivity [hPa]
1	23.8	Surface
2	31.4	Surface
3	50.3	Surface
4	52.8	920 - 810
5	53.596 ± 0.115	650 - 530
6	54.4	390 - 320
7	54.94	260 - 200
8	55.0	170 - 135
9	$57.29 = f_0$	85 - 70
10	$f_0 \pm 0.217$	50 - 40
11	$f_0 \pm 0.3222 \pm 0.048$	25 - 20
12	$f_0 \pm 0.3222 \pm 0.022$	10
13	$f_0 \pm 0.3222 \pm 0.010$	5
14	$f_0 \pm 0.3222 \pm 0.0045$	3
15	89.0	Surface

gained from increasing the global usage of AMSU-A channel 5 by say 10%, approximately the fraction removed by cloud screening?

The experience of all-sky assimilation at imager and humidity sounder frequencies suggests that these cloud-affected radiances can indeed have a significant impact. Observations in meteorologically active locations such as the warm conveyor belts of extratropical cyclones, or within hurricanes and deep convective clouds (Geer *et al.*, 2014), can have a larger impact on the analysis and forecast than those in clear-sky scenes that are already well constrained by other observations. For example, about half of the short-range forecast impact of the AMSR2 (Advanced Microwave Scanning Radiometer-2) microwave imager comes from the 12% of scenes that are most affected by precipitation (Boukabara *et al.*, 2020, Fig. 48.9). Another reason to assimilate AMSU-A in all-sky conditions is that temperature sounding channels contain significant and unique information content on precipitation processes (e.g. Bauer and Mugnai, 2003; Munchak and Skofronick-Jackson, 2013). Furthermore, variational data assimilation is underpinned by assumptions of Gaussian-distributed errors, and inclusion of even weak cloud influences on radiances may yield a more Gaussian and balanced distribution of departure statistics (Bauer *et al.*, 2010; Geer *et al.*, 2012). Thus it has been the stated goal for several years that ECMWF gradually move all microwave assimilation to the all-sky paradigm.[1]

Aside from the usual challenges of cloud and precipitation assimilation reviewed/summarised by Errico *et al.* (e.g. 2007), the difficulty of moving AMSU-A to all-sky assimilation lies in three related factors that are unique to temperature sounders and in contrast to previous activations of microwave sensors in all-sky conditions. First, the clear-sky assimilation of AMSU-A data has been developed and refined over many years, so a preliminary all-sky configuration may not be able to replicate the forecast impact of the clear-sky observations; further, some refinements of the clear-sky assimilation may be difficult to implement in the all-sky framework, either for technical or scientific reasons. Second, the percentage of observations that can truly benefit from all-sky treatment (i.e. those previously rejected) is limited. The limited additional observations exist primarily in regions where modelling and radiative transfer are most challenging; this may make it hard to see a significant signal in experimentation, and the chal-

[1]https://www.ecmwf.int/en/annual-report-2015/advancing-weather-science

lenging locations require that the error model is well tuned. Third, the radiative signal for atmospheric temperature increments is on the order of tenths of a degree (e.g. Bell *et al.*, 2008), whereas errors from scattering radiative transfer or misplaced convection can be tens of degrees. This places great pressure on the assimilation system to differentiate signal from noise and must ensure that increments are applied to the correct variable (Geer *et al.*, 2012).

Some NWP centres have prioritised the development of all-sky temperature sounding. These centres now have operational all-sky assimilation of AMSU-A (and in one case its successor, ATMS; Zhu *et al.*, 2016, 2019; Migliorini and Candy, 2019). However, these were systems with less extensive pre-existing assimilation of microwave imaging and humidity sounding channels, and no other sensors were being assimilated in all-sky conditions (see Geer *et al.*, 2018, their Table 3). Hence the newly added cloudy scenes, and particularly the new information on cloud and humidity, may have brought unique new information into those systems. By contrast, the ECMWF Integrated Forecasting System (IFS) already assimilates around 10 microwave imagers and humidity sounders in all-sky conditions. Hence the potential benefit or signal from moving AMSU-A to all-sky may be more limited. Another point of difference is the set of channels being assimilated. Following Weston *et al.* (2019), the approach in this work is to fully replace the clear-sky methodology with that of all-sky, and hence AMSU-A channels 5 to 14 are all included in the all-sky framework. In contrast, Migliorini and Candy (2019) activated just channels 4 and 5 in the all-sky framework. Zhu *et al.* (2016) activated not just the temperature-sounding channels of AMSU-A, but the imaging channels as well. These surface-sensitive channels have not been considered in the current implementation because their information content is likely similar to the many microwave imagers that are already assimilated (see e.g. Geer *et al.*, 2012). One potential advantage in the current work is that precipitating scenes, including deep convection, are actively assimilated. At other centres with all-sky AMSU-A assimilation, these scenes were initially excluded because precipitation variables were not available in the data assimilation frameworks. NCEP have now extended their system to assimilate precipitation variables, with some positive impact on short-range forecasts, but due to limitations in the scattering radiative transfer, deep convective scenes are still excluded (Tong *et al.*, 2020). The outsize impact of precipitating scenes in the all-sky microwave imager assimilation at ECMWF also strongly motivates the inclusion of such scenes.

While the focus here is on AMSU-A, these developments will be extended to current and future temperature sounders, including the Advanced Technology Microwave Sounder (ATMS), Micro-Wave Sounder (MWS), and others.

2 Methods

Table 2 summarises the clear-sky and all-sky frameworks for assimilating AMSU-A at ECMWF; these are the result of several years of parallel development. Key elements of the all-sky methodology for microwave imagers and humidity sounders (Geer and Bauer, 2010; Geer *et al.*, 2014) are the treatment of scattering and emission from clouds and precipitation in the radiative transfer, relative lack of data pre-selection, and treating representation errors caused by clouds as part of the situation-dependent observation error model. These are all retained in the implementation for temperature sounders. However, many aspects of the clear-sky assimilation strategy have been adopted for all-sky AMSU-A, and indeed this has proved crucial in getting good results. These aspects include the channel selection, bias correction models, constrained bias correction for channel 14 (Han and Bormann, 2016), and slant-path radiative transfer (Bormann, 2017). This section details only the key developments that have enabled successful transition from clear-sky to all-sky assimilation. Further information can be found in earlier reports on the development of all-sky AMSU-A assimilation (Geer *et al.*, 2012; Weston *et al.*, 2019) and

other citations within the table.

2.1 Data selection

A key element of successful all-sky AMSU-A assimilation has been to ensure that data sampling in clear-sky conditions, and in the stratospheric channels, remains very similar (Weston *et al.*, 2019). A first aspect of data selection is thinning, which is used primarily to reduce the effect of spatial observation error correlations that are otherwise not accounted for in the assimilation system. In the clear-sky assimilation of AMSU-A, thinning is applied in 125 km boxes, selecting the TB vector most likely to be viewing a clear scene, ascertained by a departure check. With several AMSU-A sensors active at once, it is also imperative to thin the different satellites together, and this is done using time slots of 30 minutes within the larger assimilation window.

For the all-sky AMSU-A assimilation, a main difference is that data are selected for the location nearest to a grid point on a Gaussian grid, and without superobbing, similar to the treatment of all-sky microwave sounders like the Microwave Humidity Sounder (MHS) (Geer *et al.*, 2014). The preference for observations that are likely cloud-free is removed. However, it proved important to retain an approximately 125 km spacing, like the clear-sky treatment; this was achieved by using a TL159 grid (all-sky MHS uses an alternative grid and thinning pattern). Additional experiments showed considerable sensitivity to the thinning approach. Results were worse not just when fewer observations were assimilated overall, but also when total observation numbers were similar but the distribution was different, such as when stratified by latitude or scan position. In the higher-peaking channels, the final choice of TL159 thinning results in a similar total data volume, and a similar latitude and scan-position distribution as used previously.

Excluding the screening of cloud and precipitation, other aspects of data selection are broadly the same between the clear-sky and all-sky frameworks (Table 2). As in clear-sky, the outermost scan positions are screened out due to strong bias characteristics, and the more surface-sensitive channels are screened for high orography, Antarctica, and mixed scenes (i.e. coastlines). Scenes where the surface emissivity or other characteristics may be in error are excluded using a channel 4-based departure check; however, this is applied only over frozen surfaces (likely snow and sea-ice) in the all-sky AMSU-A framework, rather than all land and sea-ice scenes.

2.2 Radiative Transfer

The largest hydrometeor impact on AMSU-A brightness temperatures is from the ice, snow, hail, graupel and other particles (including mixed phase) in deep-convective clouds. The first attempts at assimilating AMSU-A in clouds and precipitation were limited by a poor representation of scattering radiative transfer in these areas (Geer *et al.*, 2012). This required screening out such scenes and limited the overall efficacy of all-sky assimilation. The situation has improved due to steady progress in the modelling of scattering within the radiative transfer solver used for all-sky microwave assimilation at ECMWF, RTTOV-SCATT (Radiative Transfer for TOVS microwave scattering package, Bauer *et al.* (2006)). Improved ice scattering in RTTOV-SCATT enabled better simulation of frequencies used by temperature sounders (Geer and Baordo, 2014); further detail on recent developments in RTTOV-SCATT is given by Geer *et al.* (2017). Thus AMSU-A radiances no longer need to be screened for deep convection. Results presented in this paper use RTTOV and RTTOV-SCATT v12.1 (Saunders *et al.*, 2018).

The specification of surface emissivity is similar for the clear-sky and all-sky systems: surface emissivity

	Clear-sky (CS)	All-sky (AS)
RT model	RTTOV v12.1 (Saunders *et al.*, 2018)	RTTOV-SCATT v12.1 (Bauer *et al.*, 2006; Geer *et al.*, 2009)
Gas species	Gases (O2, N2, O3, H2O)	As CS
Hydrometeors	None	Cloud liquid, cloud ice, snow, rain (convective and large-scale precipitation included) (Geer and Baordo, 2014)
Skin temperature sink variable	Yes	No
Ocean emissivity	FASTEM-6 emissivity model (Kazumori and English, 2015)	As CS
Land/sea-ice emissivity	Dynamic emissivity retrieval using Ch3 (Karbou *et al.*, 2006)	As CS but using all-sky dynamic retrieval (Baordo and Geer, 2016)
Land/sea-ice emissivity/skin-temperature screening	Ch4-based departure check (Ch5-7)	As CS, but only over sea-ice and likely snow
Screening for orography	Based on rejecting observations with large observation-error estimates (Lawrence *et al.*, 2015)	Tropics ($< 30°$): Ch5 1000m, Ch6 2000m; Extratropics: Ch5 500m, Ch6 1500m
Antarctica screening	No Ch5 over land or sea-ice south of 60°S	As CS
Coasts (Chs. 5-6)	Land 1-50% screened out, 50+% treated as land	As CS
Cloud screening	Mixture of LWP, SI, and departure checks (Chs. 5-8) (Weston *et al.*, 2019, Table 2)	None, apart from SI $>$ 20K removed over land
Observation errors	Noise, cloud- and surface-dependent (Lawrence *et al.*, 2015)	Noise and cloud-dependent (Geer and Bauer, 2011); scan position dependent (Geer *et al.*, 2012); adjusted settings in clear-sky situations (see text)
Thinning resolution	125 km boxes	Approximately 125 km boxes based on T_L159 reduced Gaussian grid
Thinning strategy	All satellites together in 30min windows; select most-likely clear radiance	As CS, but select observation closest to grid box centre
Scan position	Reject outer-most scan positions on each side (1-3, 28-30)	As CS
Quality control	First guess check and VarQC (Andersson and Järvinen, 1999)	As CS but using cloud-dependant obs. error model and with adjusted settings (see text)
Bias correction	VarBC with constant, air mass, and third order polynomial scan predictors; constrained VarBC for channel 14 (Han and Bormann, 2016)	As CS
Interpolation	Bi-linear/bi-cubic; slant-path (Bormann, 2017)	As CS but with nearest-neighbour interpolation for hydrometeors

Table 3: Summary of the assimilation configuration for the clear-sky and all-sky systems. Further details in the text and referenced literature.
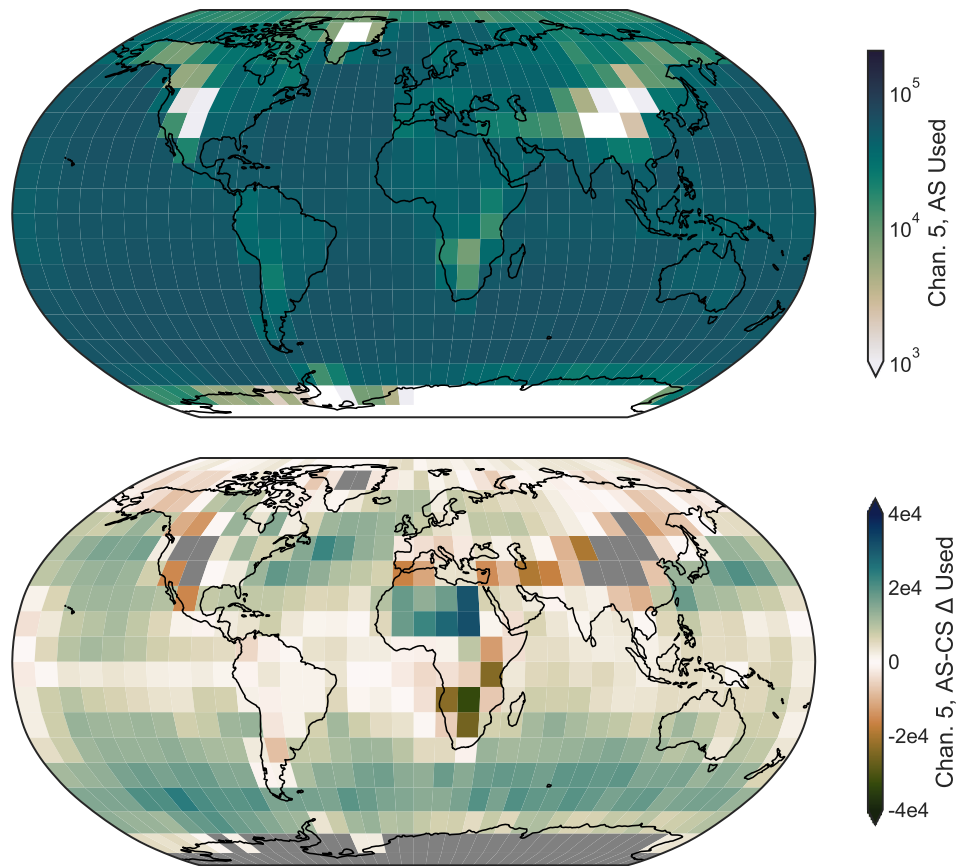
Figure 1: Used channel 5 observations from all sensors combined, December 2019 to March 2020. Shown are all-sky observation counts (top) and all-sky minus clear-sky counts (bottom), where areas in grey indicate one experiment has fewer than 1000 observations used.

over sea comes from the Fast microwave Emissivity Model (FASTEM-6; Kazumori and English (2015)); over land, a dynamic emissivity retrieval is performed for each scene using channel 3, the most surface-sensitive of the 50 GHz channels. One key difference between clear-sky and all-sky is the treatment of skin temperature. In the clear-sky system, a "sink variable" is used to retrieve a separate skin temperature for each field of view as part of 4D-Var, with the background provided by the model surface temperature. The retrieval is subsequently discarded after the assimilation. In all-sky, the skin temperature sink variable is not used so as to avoid cloud increments being ascribed to the surface. The model surface temperature is taken as effective skin temperature, with the dynamic emissivity retrieval partially accounting for possible skin temperature errors. To avoid signals due to poor skin temperature estimates aliasing into atmospheric increments over snow-covered land or sea-ice surfaces, screening is applied using a departure check on channel 4, adapted from the clear-sky system. In addition, screening for orography is more conservative in all-sky lest poor skin temperatures or emissivities are aliased into atmospheric increments (Bormann *et al.*, 2017). Areas of ongoing research involve the treatment of surface emissivity for scenes with multiple surface types and two-dimensional treatment of skin temperatures (Massart *et al.*, 2021).

Figure 1 compares used data counts for channel 5 between the all-sky and clear-sky systems. As a result of the aforementioned differences over land for lower-peaking channels (5 and 6), more observations are used over desert regions in all-sky but fewer data are assimilated over large mountain ranges. The

increase is on the order of 30-40% over sea in the mid-latitude storm track regions.

2.3   Observation Error Modelling

At the heart of all-sky assimilation is the observation error model, driven by the so-called symmetric cloud predictor (Geer and Bauer, 2011). The all-sky error model incorporates a base level of error, applicable to clear-sky scenes and primarily accounting for instrument noise. Larger forward model and representation errors in cloudy scenes are modelled by using a proxy for cloud amount to scale the error values in a situation-dependent manner. Error contributions arising from hydrometeors in either the observed field of view or that of the model background are balanced equally, as either of these could cause discrepancy between observed and modelled radiances. Through the symmetric error model, representation errors and forward model errors are wrapped up with sensor noise and given as a total observation error. Parameters governing the error model are derived from standard deviations of background departures, binned by the cloud proxy.

Cloud proxies vary for different microwave sensors, as the optimal proxy depends on the channel sensitivities as well as the information content available. Whereas imagers use a polarisation difference at 37 GHz to primarily identify scattering from precipitation, humidity sounders use a "scattering index" (SI) formed by two higher frequency channels near 90 and 150 GHz that is primarily sensitive to frozen hydrometeors aloft. Depending on the sensitivity of the channel, the error model may use a linear, quadratic, or mixed linear-quadratic relationship between the assigned error and the cloud proxy. Two tie points are given, one for clear and one for fully cloudy.

AMSU-A has a channel suite unlike imagers or humidity sounders, and therefore different cloud proxies are needed. Over sea the cloud proxy is a liquid water path (LWP) retrieval based on Grody *et al.* (2001), using brightness temperature (TB) from channels 1 and 2. This is a variation on a typical split-window approach, using a regression to homogenise the result regardless of scan position and provide a line of sight LWP estimate. Equation 1 is a function of zenith angle (θ) and given in terms of kg/m^{-2}, i.e. *mm* of liquid water:

$$LWP = 8.24 - cos(\theta)(2.539 - 1.744cos(\theta)) + 0.754ln(285 - TB_1) - 2.265ln(285 - TB_2). \quad (1)$$

The same approach was used by Geer *et al.* (2012), Zhu *et al.* (2016), Migliorini and Candy (2019) but with a multiplication by $cos(\theta)$ to retrieve the vertical column LWP. Here also the 2nd and 3rd coefficients have been updated compared to Grody *et al.* (2001); further details are in Geer *et al.* (2012).

Over land a scattering index formed by a difference of channels 1 and 15 provides the cloud proxy:

$$SI = TB_1 - TB_{15} \quad (2)$$

This copies the approach of humidity sounders but with the error proxy more sensitive to precipitation than frozen hydrometeors aloft, befitting the different sensitivity of AMSU-A channels. Examples of the error model are seen in Figure 2 for channels 5 and 6.

The error model over sea is modified to account for the differential cloud sensitivity of observations across the scan. The nadir view sees deeper into the atmosphere and is more likely to encounter precipitation or surface sensitivity. This is handled by scaling the error model output according to scan position, using the following scaling factor, dependent on the zenith angle θ:

$$f(\theta) = 0.3 + 0.7exp(-\frac{\beta^2\theta^2}{2}) \quad (3)$$
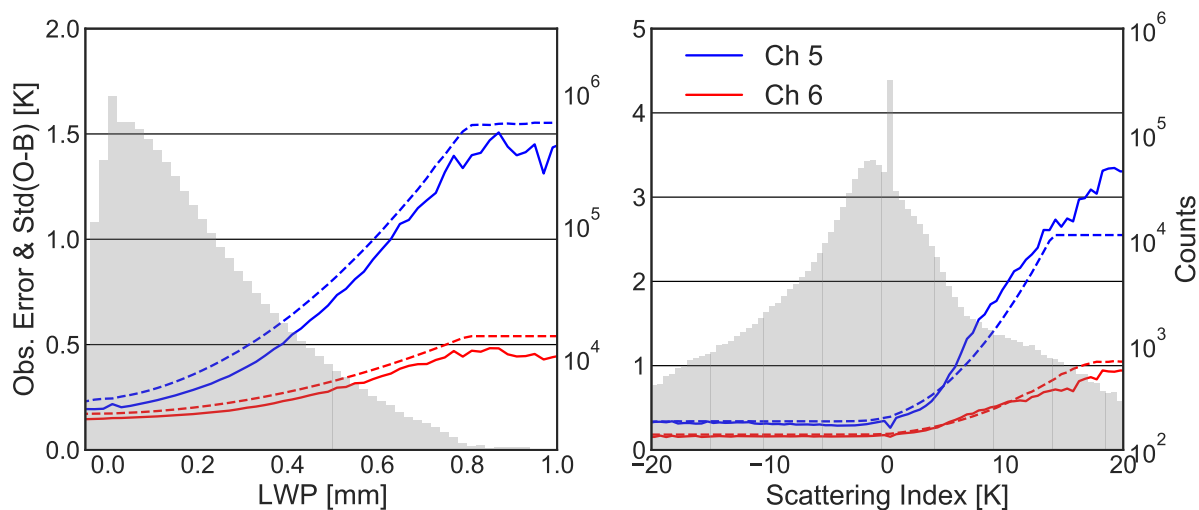
Figure 2: Observation error models (dashed) and standard deviation of background departures (solid) for channels 5 and 6 over sea (left) and land (right). Data comprise a month of used observations from all AMSU-A sensors combined, March 2020.

Here, β is a free parameter, derived separately for each channel to achieve a flatter distribution of normalised departures. The functional form of the scaling has been derived empirically, and it is applied to channels 3-5 only (with $\beta_3 = 1.4$, $\beta_4 = 1.7$, $\beta_5 = 0.9$). Exemplifying the need for this scaling, Figure 3 shows channel 5 departure statistics by scan position. Assigned observation errors are greater near the scan's midpoint, yielding normalised departures without a strong dependence on scan position. This effect is stronger in cloudy scenes, as shown in the figure. The error adjustment is not applied over land or for higher peaking channels as the angular dependence of normalised departures is not as strong.
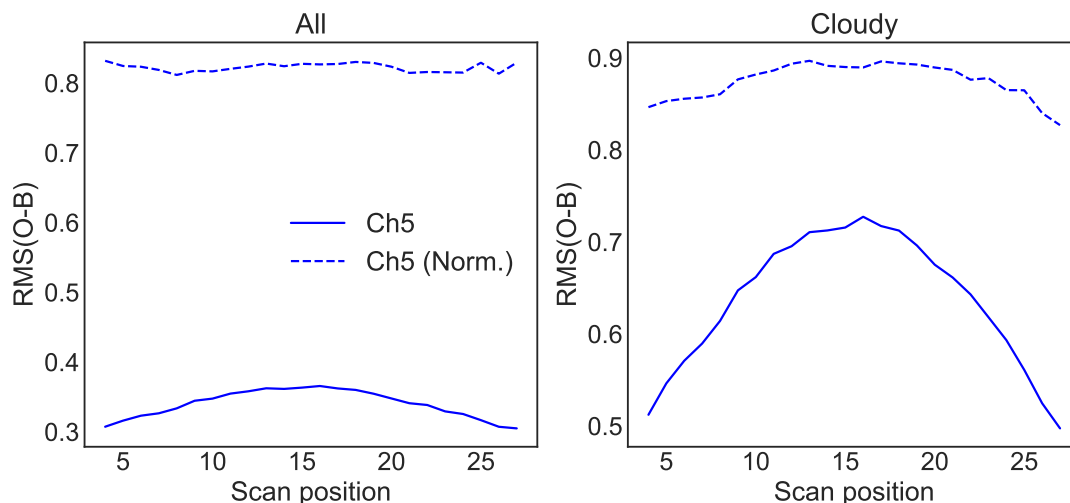

Figure 3: Mean RMS of first guess departures (in Kelvin) and normalised first guess departures (unit-less) for AMSU-A channel 5 over sea, as a function of sensor scan position. Statistics are for used data from one month. All data are considered on the left, whereas on the right it is just observations that indicated likely cloud, symmetric $LWP > 0.15 kgm^{-2}$.

Application of the all-sky error model is only relevant for AMSU-A channels with tropospheric sensitivity, namely those with sensitivity to cloud. Hence the error model is applied to channels 9 and below.

Table 4: Clear-sky and all-sky error model values are given for Metop-C AMSU-A as an example (all in Kelvin), along with a priori probabilities of gross error (A).

	Clear-sky		All-sky				
	Error	A	Clear (sea)	Cloudy (sea)	Clear (land)	Cloudy (land)	A
5	0.27	0.050	0.24	1.70	0.33	2.55	0.200
6	0.18	0.050	0.17	0.54	0.18	0.90	0.100
7	0.19	0.003	0.18	0.25	0.19	0.45	0.020
8	0.20	0.003	0.19	0.21	0.20	0.27	0.010
9	0.19	0.003	0.19	0.22	0.20	0.27	0.003
10	0.24	0.003	0.25	-	0.25	-	0.003
11	0.34	0.015	0.34	-	0.34	-	0.015
12	0.50	0.015	0.50	-	0.50	-	0.015
13	0.81	0.015	0.84	-	0.84	-	0.015
14	1.40	0.050	1.40	-	1.40	-	0.050

For each channel and surface type (currently sea or land), the choice of error model shape (as a function of the cloud predictor) is driven by the sensitivity of departures to cloud proxy. Channels 5 and 6 employ quadratic shapes over sea and land. For higher-peaking channels the response is more linear, and a linear model is used for channel 7-9 over sea; only channel 9 uses a linear model over land, whereas channels 5-8 use a quadratic model (see Fig. 2).

Lastly, several AMSU-A sensors possess broken channels (see Table 1). Some of these are channels used in the error model, and this disables the active, all-sky assimilation of tropospheric channels on these particular platforms. For example, Metop-B has a broken channel 15 and this precludes all-sky use of its tropospheric channels over land. Due to limitations wrought by broken channels, each AMSU-A is not equal when it comes to all-sky impact. For example, the AMSU-A on Metop-C can have a large impact on the analysis due to its lack of broken channels, whereas Aqua AMSU-A lacks functioning channels to enable all-sky usage over ocean or land.

2.4   VarQC and Observation Errors

Variational quality control (VarQC, Andersson and Järvinen, 1999) modifies the weight that observations receive in the 4D-Var cost function to ensure that probability density functions (PDFs) of analysis departures are more Gaussian with fewer outliers. This is done by estimating the *prior* probability of gross error (PGE) during the assimilation, that is the probability that the error in the observation belongs to a white-noise rather than a Gaussian distribution. This requires the specification of an *a priori* probability of gross error (PGE), and the *posterior* PGE is then a function of the analysis departure. The weight given to an observation is inversely proportional to its posterior PGE, so observations with a high *posterior* PGE have little impact on the analysis. VarQC is applied to a wide range of observation types during the assimilation. The procedure is crucial for all-sky assimilation (Bauer *et al.*, 2010; Geer and Bauer, 2011; Zhu *et al.*, 2016) as it helps to minimise over-fitting to outlying observations. VarQC acts in concert with other quality control procedures to trim the PDF of all-sky observations to make them more readily assimilated (see Fig. 2 in Geer *et al.*, 2014).

In all-sky assimilation, VarQC settings for AMSU-A are notably different for tropospheric channels (see Table 4). Whereas clear-sky AMSU-A uses a near-zero *a priori* PGE (here denoted *A*), larger values are

called for when treating the lower peaking channels that see clouds and precipitation. This is primarily due to more significant tails to the distribution for analysis departures of non-clear observations.
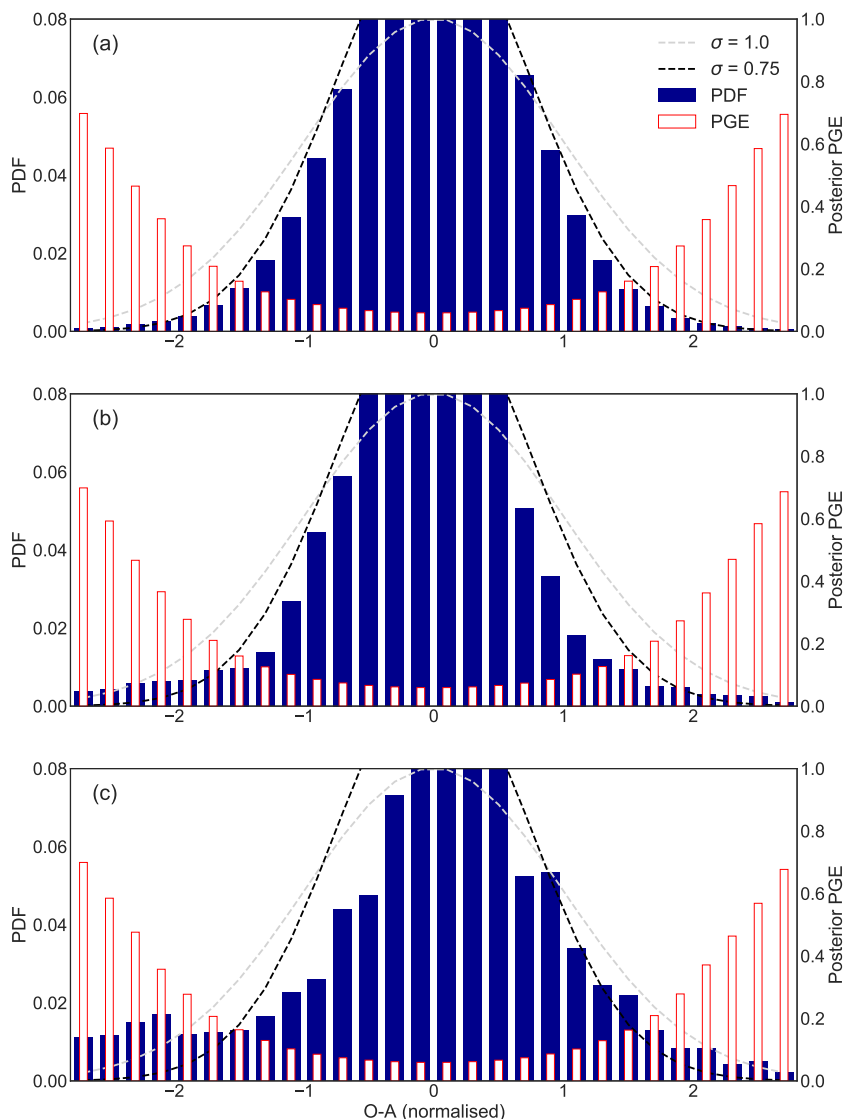

Figure 4: PDFs of analysis departures (observed minus analysis) and posterior probabilities of gross error for ten days of Metop-C data in September 2020. Used channel 5 data are shown for observations in all conditions (a), cloudy over sea (b), and cloudy over land (c). Here "cloudy" is defined as $LWP > 0.3 kgm^{-2}$ over sea and $SI > 3K$ over land.

Figure 4 shows PDFs of normalised analysis departures (i.e. O-A) from channel 5 on Metop-C, spanning ten days of used data in September 2019. The departures are normalised by the assigned observation error, as per Fig. 2. The *posterior* PGE is also given for each departure bin, indicating which observations received less weight in the analysis (weight is defined as $(1 - PGE)$). As PGE is solely a function of normalised analysis departure and A, data on the wings receive little weight in the analysis; however, it is crucial to note that even near-zero analysis departures have non-zero *posterior* PGE due to the prescription of A (Andersson and Järvinen, 1999, Eqs. 12, 14). Gaussian curves are given in Fig. 4 to aid judgement of the distributions' Gaussianity. The top plot shows all used data, while the bottom two plots focus on "cloudy" observations that are rejected in clear-sky, namely those with $LWP > 0.3$ mm over sea

(middle) and *SI* >3 K over land (bottom). These cloudy PDFs possess more significant tails, exactly the type of behaviour that VarQC can help to ameliorate. The cloudy PDFs are more peaked and greater residual bias is also visible, especially for cloud-affected radiances over land.

The cloudy departure PDFs offer a compelling reason to apply a non-zero *a priori* PGE for tropospheric channels that are sensitive to cloud, precipitation, and surface emission. In comparison, the *A* values used for imager and humidity sounder channels assimilated in all-sky at ECMWF are usually in the range $0.3 \leq A \leq 0.5$. Trial and error in earlier testing of all-sky AMSU-A configurations led to intermediate *A* values chosen for AMSU-A, with channels 5 and 6 set to $A = 0.2$ and $A = 0.1$, respectively. There is no objective method to determine such values, but these are decidedly in between those of wholly clear-sky channels and higher-peaking humidity sounding channels.

A key aim in moving AMSU-A to all-sky is to retain its clear-sky impact on the analysis, but the first attempts to tune VarQC resulted in minor tropospheric degradations because there was no corresponding adjustment to the observation error model. To ensure that AMSU-A observations retained their impact in clear skies despite VarQC adjustments, the observation errors were adjusted to conserve the total analysis impact as measured by the 4D-Var cost function. Using Eq. 9 from Andersson and Järvinen (1999), increasing *A* from 0.05 to 0.20 required approximately a 15% reduction in the error values for channel 5. Channel 6 errors were modified less, as changing *A* from 0.003 to 0.10 was offset by about a 10% error reduction. This decision-making led to the values given in Table 4. It is a balancing act to lessen the influence of outliers from cloudy observations whilst retaining the clear-sky sounding impact, but these changes to VarQC treatment have shown significant improvement in AMSU-A assimilation in regions of deep convection and also over land.

2.5 Experiments

The all-sky approach outlined above is investigated in three assimilation experiments which differ only in the use of AMSU-A observations:

- **No AMSU-A**: All AMSU-A radiances removed from assimilation, but otherwise a full observing system is used

- **Clear-sky**: AMSU-A assimilated in clear-sky conditions only (active in Cycle 47R1 and before)

- **All-sky**: AMSU-A assimilated in all-sky conditions (active as of Cycle 47R3)

The experiments allow an evaluation of the overall AMSU-A impact in clear-sky or all-sky assimilation, as well as a direct comparison of the results from the two approaches.

All experiments presented use the ECMWF IFS Cycle 47R1 (ECMWF, 2020) and cover two seasons (July to November 2019 and December 2019 to March 2020), unless noted otherwise. All experiments employ incremental 4D-Var with 12hr delayed cutoff assimilation cycles. Background errors come from the operational ensemble of data assimilations (EDA) and thus represent a flow-dependent background error; this is the same for all experiments despite the observing system change, but is not expected to affect the results' interpretation (Duncan *et al.*, In press). The forecast model resolution is TCo399 (approx. 29km) L137, while the final incremental analysis resolution is TL255 (approx. 78km) L137.

3 Results

We will now assess the impact of the all-sky assimilation of AMSU-A. We will first compare the Clear-sky and the All-sky experiment against the No AMSU-A experiment, respectively, in order to put the changes between the two approaches in context to the overall impact of assimilating AMSU-A data. We will then directly compare results from the All-sky and Clear-sky experiments to highlight the benefits brought through the all-sky usage. Lastly, the impact of assimilating temperature sounding information in cloudy regions is exemplified by examination of tropical cyclones.

3.1 Replicating Clear-sky Impact

First we compare to a depleted observing system with no AMSU-A observations assimilated, in which all else is held constant (**No AMSU-A**). The change in short-range forecast skill is best assessed via independent observations. Figure 5 shows the change in background departures caused by assimilation of AMSU-A via both methods. The all-sky assimilation shows a similar impact on the background fits of infrared, microwave, and radiosonde observations. Fits in the stratosphere and troposphere witness about the same overall impact from AMSU-A regardless of the assimilation strategy. The magnitude of the impact appears quite similar in observation space, but there are some comparatively small differences that will be elaborated on in the following section.
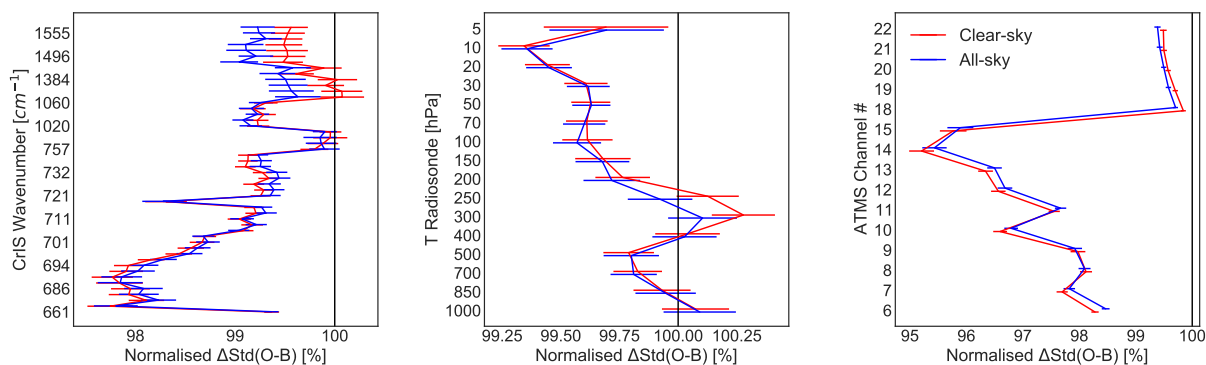

Figure 5: Change in standard deviation of observed minus background for infrared sounding (Cross-track Infrared Sounder (CrIS), left), radiosonde temperature (centre), and another microwave sounder (ATMS, right) relative to the depleted system with no AMSU-A data assimilated, given as a percent difference. All used global data are considered. Horizontal lines show confidence intervals at the 95% confidence level. For CrIS, only every third channel is shown to aid interpretation. The period spans July to September 2019 and December 2019 to March 2020.

Looking at longer forecast ranges, Figure 6 gives the change in forecast scores for three parameters at three pressure levels from lead times of 1 to 7 days. Both assimilation strategies have a similar impact on the variables and atmospheric levels examined here. Some benefits are apparent from all-sky, and these will be discussed further in the next sub-section. This is a similar picture almost independent of level or variable examined, with little discernible difference in most forecast scores.

In summary, comparisons to a baseline with no AMSU-A data show that AMSU-A has a strong impact when assimilated through either the clear-sky or the all-sky approach, and the differences from the two approaches are comparatively small. Some benefits are apparent from the all-sky assimilation and we will examine these in detail with more direct comparison next.
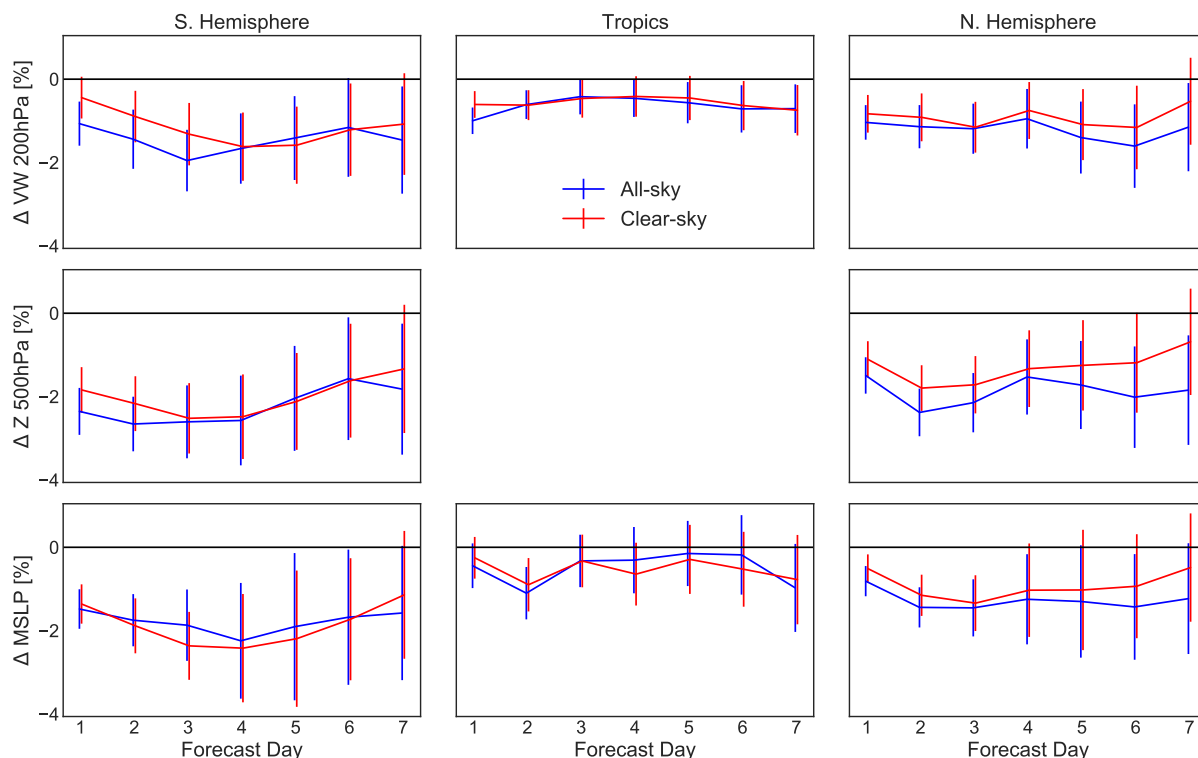
Figure 6: Forecast score changes for RMSE of vector wind (VW) at 200 hPa *(top), geopotential height at* 500 hPa *(middle), and surface pressure (bottom) for the Southern Hemisphere (90S-20S, left), Tropics (20S-20N, centre), and Northern Hemisphere (20N-90N, right). Vertical lines give 95% confidence intervals. Verification is from own analysis.*

3.2 Additional Information from All-sky

Figure 7 gives the change in background departures for some conventional and satellite-based observations, comparing all-sky AMSU-A (**All-sky**) directly against the experiment using approximately the configuration of the current operational system (**Clear-sky**). As in the previous section, infrared humidity channels show a slight improvement in fits due to all-sky microwave temperature sounding, whereas the tropospheric temperature channels of IASI (Infrared Atmospheric Sounding Interferometer) show a mostly neutral response. Radiosondes show a slight improvement in the upper tropospheric temperature, a signal at 300 hPa that appears in the tropics and extratropics. The neutral signal for temperature in the stratosphere against radiosondes or high-peaking IASI channels is expected, as all-sky usage should have little effect on the stratospheric channels of AMSU-A.

ATMS has very similar channels to AMSU-A, but is used in the clear-sky system in both experiments and shows a small unexpected degradation for the stratospheric temperature channels. This is thought to be due to subtle differences in the layering adapted in the clear-sky and the all-sky radiative transfer model used for AMSU-A. As no other observations sensitive to temperature in the stratosphere show a similar feature (e.g. radio occultation departures are neutral), it is not considered a concern. The slight apparent degradation against the lowest ATMS temperature channels (6 and 7) is also not backed up by other observations with similar sensitivity. It is likely a result of ATMS being used in the clear-sky system in both experiments, hence favouring the error characteristics of the clear-sky AMSU-A assimilation; the nearly identical spectral response of many channels on ATMS and AMSU-A means that the different

assimilation strategy and correlated forward model errors cast some doubt on the independence of ATMS observations for verification.
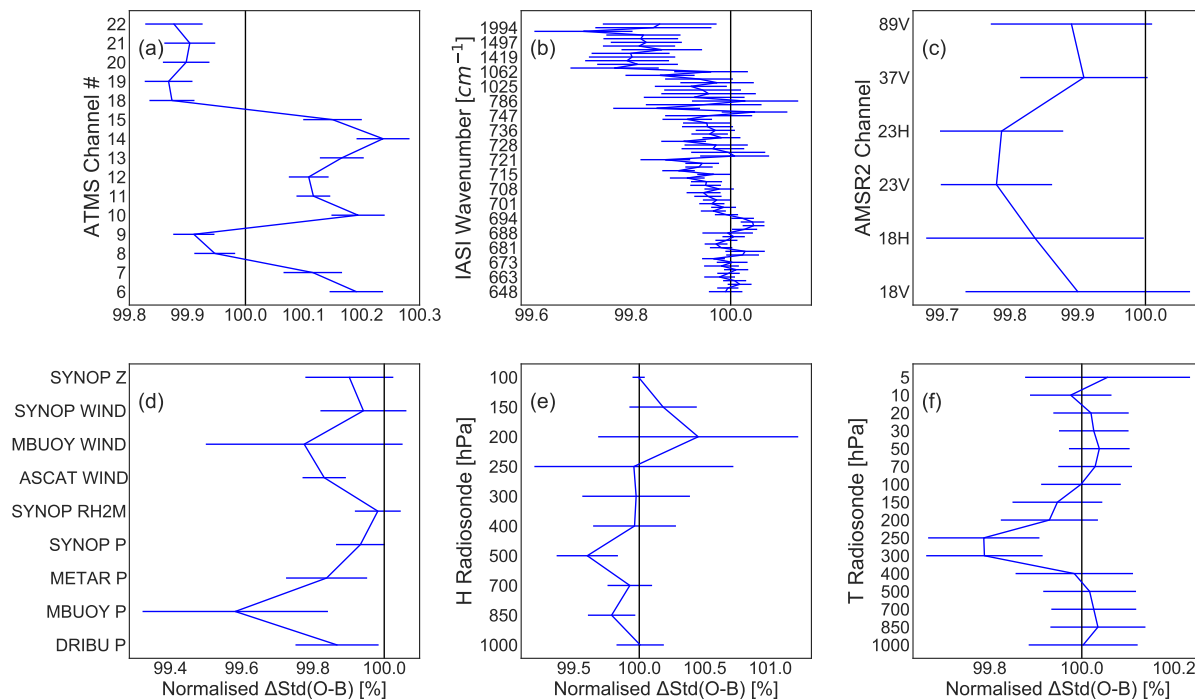

Figure 7: Changes in the background fits to observations are shown for global ATMS radiances (a), IASI radiances (b), AMSR2 radiances (c), surface-based conventional observations (d), radiosonde humidity (e), and radiosonde temperature (f). For IASI, only every third channel is plotted to aid interpretation. Confidence levels of 95% are given by horizontal lines.

Short-range forecasts of humidity are improved by all-sky AMSU-A. This is seen consistently for a number of observations, such as ATMS humidity sounding channels (18-22, Fig. 7a), IASI humidity channels (wavenumber $> 1000 cm^{-1}$, Fig. 7b), and water vapour radiances from geostationary instruments (not shown). The impact on humidity is not necessarily an intuitive result, as channel 5 has only a weak direct sensitivity to atmospheric humidity, i.e. through the Jacobian for humidity, which is about 100 times weaker than for 183 GHz channels. Instead, this may be an effect of interplay between clouds and humidity via the 4D-Var tracer effect (Peubey and McNally, 2009), and could explain the improvement in background fits for some microwave imager channels as well. Specifically, while most microwave imager channels showed a neutral response, the 23 GHz channels on GMI (Global Precipitation Measurement Microwave Imager), AMSR2, and SSMIS (Special Sensor Microwave Imager/Sounder) all showed tighter background fits caused by all-sky AMSU-A assimilation, indicating an improvement to column water vapour (seen for 23 GHz channels of AMSR2 in Fig. 7c). This is in line with Lawrence *et al.* (2018), who found signals of improved cloud fields from assimilating the 118 GHz temperature sounding channels on MWHS-2 (MicroWave Humidity Sounder 2) in all-sky conditions. The all-sky use of AMSU-A might also allow better separation of otherwise ambiguous signals from sources such as humidity sounding channels on other sensors, allowing humidity, cloud, and temperature signals to be better disentangled via their synergy in 4D-Var.

Surface-based conventional observations also show some benefit from all-sky AMSU-A. In the tropics especially, fits to surface pressure measurements from moored buoys, SYNOP stations, and drifting buoys all show a significant improvement (Fig. 7 gives global statistics, but most buoys are in the tropics

Table 5: Forecast sensitivity to observation impact (FSOI) per channel from AMSU-A in clear-sky and all-sky assimilated observations over a four week period in September 2019. FSOI is given in $-1\,\mathrm{J\,kg^{-1}}$.

Ch.	Clear-sky			All-sky		
	No. Obs.	Mean FSOI	Total FSOI	No. Obs.	Mean FSOI	Total FSOI
5	5.31e6	0.37	1.98e5	5.89e6	0.52	3.04e5
6	5.28e6	0.72	3.80e5	5.55e6	0.64	3.57e5
7	4.86e6	0.53	2.58e5	4.82e6	0.47	2.27e5
8	6.15e6	0.57	3.48e5	6.37e6	0.51	3.22e5

and this is where most improvement is seen). Fits to the Advanced Scatterometer (ASCAT) indicate that short-range wind forecasts near the ocean surface are also improved. Taken together, this indicates a more realistic distribution of atmospheric mass over the tropical oceans due to all-sky assimilation of temperature sounding channels. This may help to explain downstream forecast impacts, as errors in the eastern tropical Pacific can result in forecast "busts" over Europe several days later, for example (Magnusson, 2017).

The impact of all-sky AMSU-A on upper air scores is explored in Figure 8, with a few lead times shown for winds and geopotential height in the mid and upper troposphere. There is broad improvement at T+24hrs, particularly over sea and in regions such as the Southern Ocean where all-sky increases the sampling significantly. This figure can be considered a complement to Fig. 6, showing the regions in which all-sky AMSU-A improves upper air scores. Some of these upper air improvements appear to persist several days into the forecast. The potential teleconnection between the eastern tropical Pacific at short ranges and Europe a week later recalls Magnusson (2017), but other improvements visible around North America may also contribute.

Figure 9 gives the change in Z500 RMSE caused by moving to all-sky AMSU-A assimilation, averaged over the northern and southern hemisphere extratropics, and also Europe. This shows that all-sky AMSU-A causes significant improvements in the middle troposphere through day 2, decreasing Z500 errors by approximately 0.5% in both hemispheres at short lead times. There is an indication that mid-tropospheric scores are significantly improved at longer lead times over Europe specifically, peaking at day 8. The mechanisms for the longer-range impact over Europe are not fully understood, though they may be a result of improvements to short-range forecasts in the eastern tropical Pacific noted above.

Another way to judge forecast impact is via the adjoint-based forecast sensitivity to observation impact, or FSOI (Cardinali, 2009); FSOI is a metric that estimates how individual observations changed the forecast and whether this was a good change based on analysis verification of a 24 hour forecast, with respect to a global dry total energy norm. Although there are many caveats for interpreting FSOI results, it is considered a useful diagnostic tool that aims to attribute forecast impact to individual observations (English *et al.*, 2020). Four weeks of FSOI statistics were compiled over the month of September 2019, separately for the all-sky and clear-sky configurations. The mean and total FSOI for the tropospheric AMSU-A channels of all satellites combined are given in Table 5. Strikingly, the total FSOI for all tropospheric channels combined is quite similar whether in clear- or all-sky usage. All-sky gets more impact out of channel 5, due to the increase in data counts and mean impact per observation, whereas the FSOI contribution of the other tropospheric channels is reduced. A plausible interpretation may be that some of the impact now attributed to channel 5 was previously partially achieved through the clear-sky assimilation of the other channels.

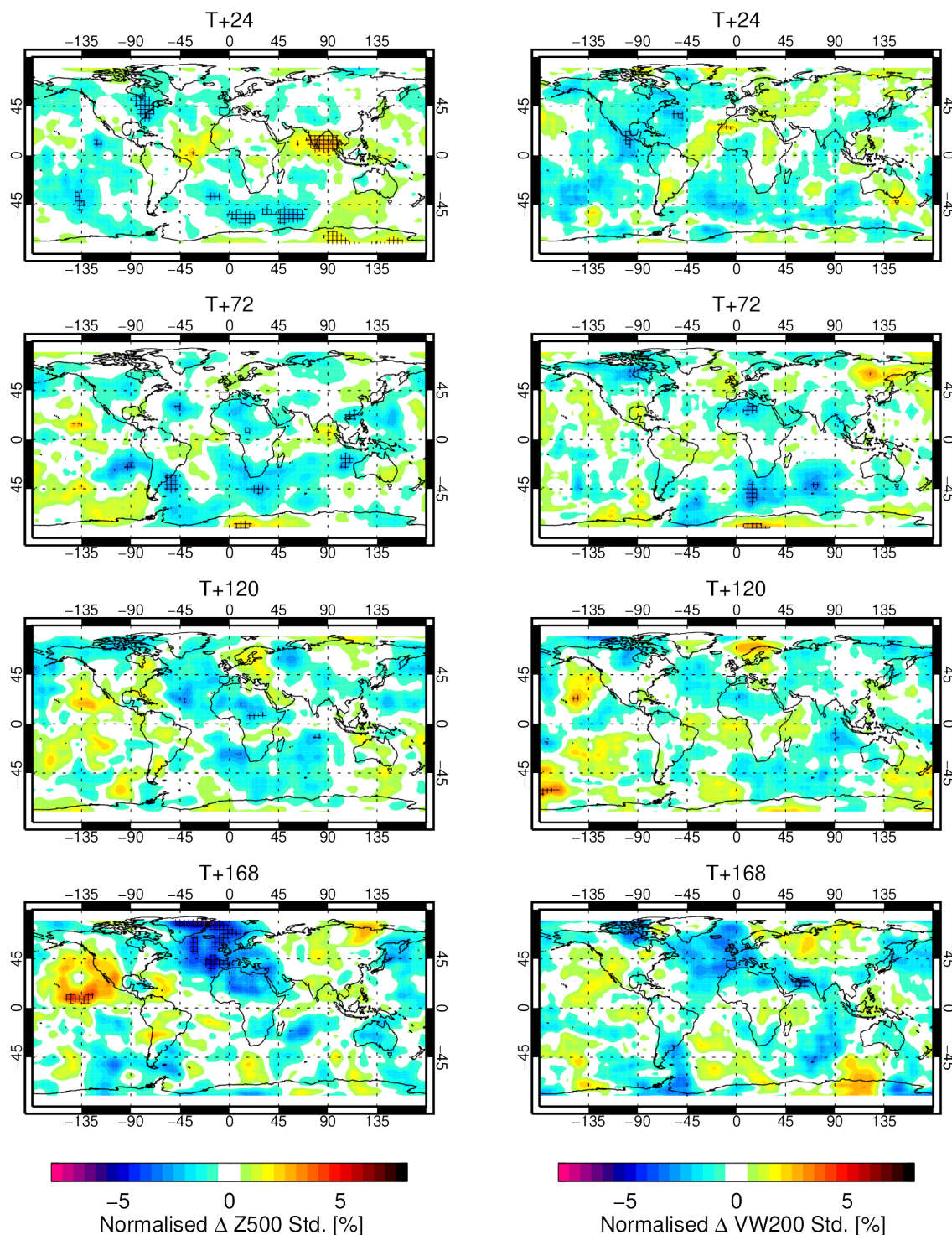The spatial distribution of global FSOI is explored in Figure 10, with channel 5 FSOI plotted for each,

Figure 8: *Maps of changes in* 500 hPa *geopotential height (left) and* 200 hPa *vector wind (VW; right) standard deviation from 24 hours to 7 days lead time, spanning nine months of experimentation comparing all-sky against clear-sky AMSU-A assimilation. Black hatching indicates significance at the 80% confidence level following* Geer *(2016). Verification is against own analysis.*

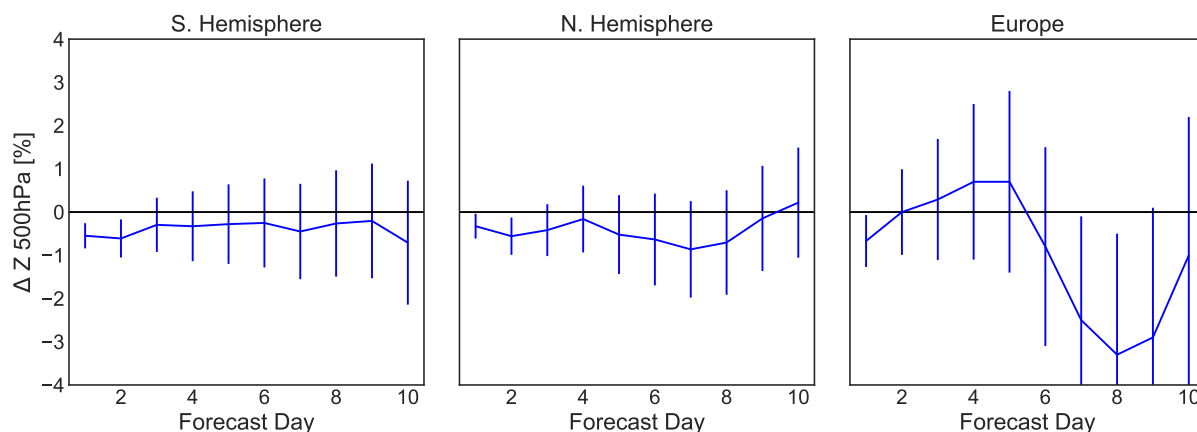alongside an integrated FSOI from channels 5-7. One notable difference is that all-sky channel 5 impact

Figure 9: Changes in Z500 RMSE averaged over the southern and northern hemisphere extratropics (poleward of 20 degrees) and Europe (35-70N, 10W-40E). Vertical bars show 95% confidence intervals following Geer (2016).

is mainly improved in the tropics and over ocean, with 90% greater impact in the tropics (30N to 30S), compared to 40% greater impact in the extratropics. In contrast, total FSOI for channels 6 and 7 retains a very similar spatial distribution, with little change in FSOI seen when comparing tropics and extratropics. The bottom panel of Fig. 10 gives the percent difference in FSOI, indicating that changes in FSOI from AMSU-A are driven by channel 5, but the total FSOI from tropospheric channels remains similar. A slight decrease in total FSOI is visible over higher latitude land regions, pointing to an area of potential future work. A few smaller, regional features from all-sky channel 5 pop out even in the totals map, such as greater impact over the Atlantic Gulf Stream, in the equatorial Pacific west of Mexico, and the north Pacific south of Alaska. Lastly, the highest FSOI seen in a single grid box is visible as a bright spot just east of Florida—this will be investigated further in the following section.

3.3 Impact on Tropical Cyclones

All-sky microwave radiances are some of the only satellite observations assimilated near the core of tropical cyclones. Numerous studies have linked temperature sounding radiances in the mid- and upper-troposhere to warm core dynamics and cyclone intensity (e.g. Brueske and Velden, 2003; Knaff *et al.*, 2004; Tian and Zou, 2016). Coincidentally, the period of experimentation contains the very active 2019 Atlantic hurricane season in which there were 20 named cyclones. In this section, we explore the impact of assimilating all-sky temperature sounding radiances near tropical cyclones, an exemplification of the greater sampling that all-sky provides for high-impact weather. We will focus primarily on two cases and the assimilation of observations both near the cyclone's centre and downstream; the relatively short period of study means that robust conclusions on the overall forecasting impact of all-sky temperature sounding on tropical cyclones are outside this paper's scope.

In the following, first we examine the season as a whole before looking at two individual tropical cyclones. This permits some explication of the earlier FSOI results from Fig. 10 as well as demonstrating how all-sky assimilation may improve representation and sampling of high-impact weather events.
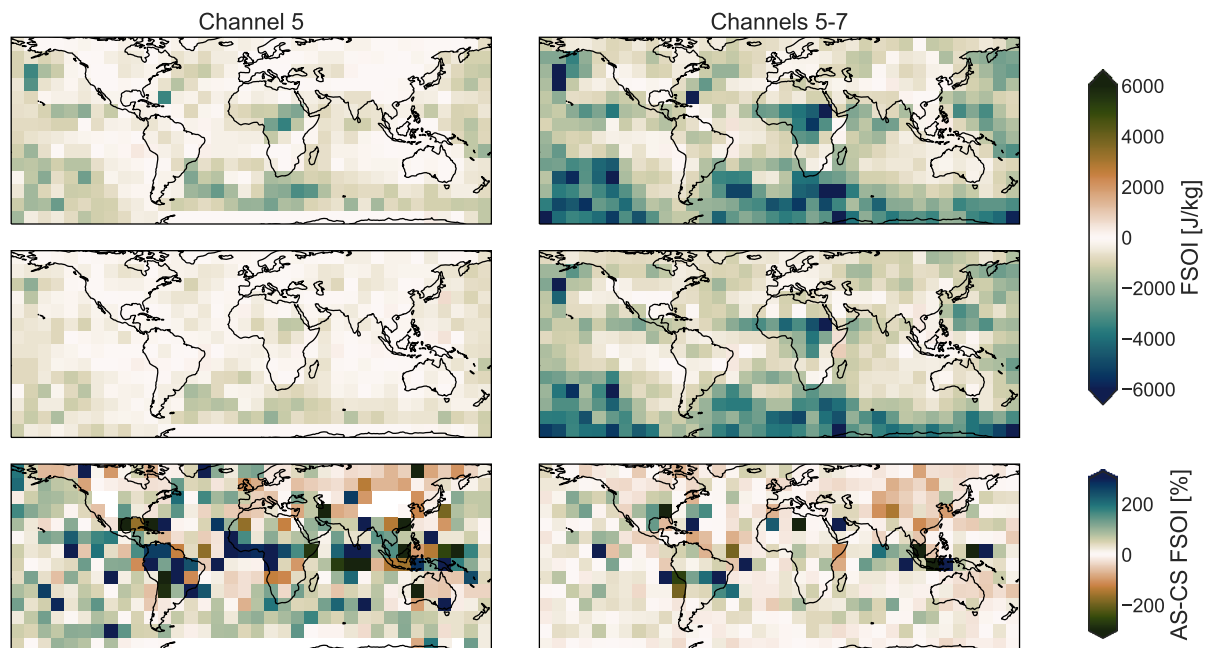
Figure 10: Monthly total FSOI maps for all-sky (top) and clear-sky (middle) and their percent difference (bottom). Channel 5 alone is shown on the left, total channel 5-7 FSOI is on the right. Data from four weeks in September 2019, averaged on a 10 degree grid. Negative FSOI indicates a beneficial impact on the 24hr forecast.

3.3.1   2019 Hurricane Season

The experimentation period includes most of the 2019 hurricane season, from July to the end of November. To examine if there was any systematic effect of all-sky temperature sounding on tropical cyclones, tracking data were analysed over the whole season, including all ocean basins (van der Grijn, 2002). Verification data come from IBTrACS (Knapp *et al.*, 2010). Results using a different verification data set were quite similar.

Figure 11 shows this verification comparison for track and central pressure errors, spanning day 0 to day 5. There is a small but fairly consistent signal in central pressure errors, with all-sky AMSU-A improving the central pressure of tropical cyclones by about 0.2 to 0.5 hPa. Verification differences for cyclone track are closer to neutral, but indicate a possible improvement at longer lead times especially. In examination of which individual tracks were most improved by all-sky AMSU-A, these appear to be cyclones that underwent significant extratropical transitions: Dorian, Humberto, Lorenzo. This is illustrated in Figure 12, with Humberto (Section 3.3.2) standing out for day 5 position errors. The figure also suggests that the cyclones with largest position errors benefit most from all-sky AMSU-A.

Any analysis of a single season for tropical cyclones is limited by the sample size. In addition, these deterministic experiments were run at relatively low spatial resolution, and thus the behaviour may differ at higher resolutions such as run in operational NWP. To this point, a separate high-resolution (9km) experiment was run for part of the 2020 hurricane season. The results showed a largely neutral impact on central pressure and position. So while the results shown here for the 2019 season are encouraging, it is too early to make strong conclusions about the impact of all-sky temperature sounding on tropical cyclones and forecast skill in general. That said, the indications of benefits are consistent with theoretical reasons why better constraint of upper tropospheric temperatures in a tropical cyclone would help forecasts (Durden, 2013; Zhu and Weng, 2013; Tian and Zou, 2016), providing plausible mechanisms
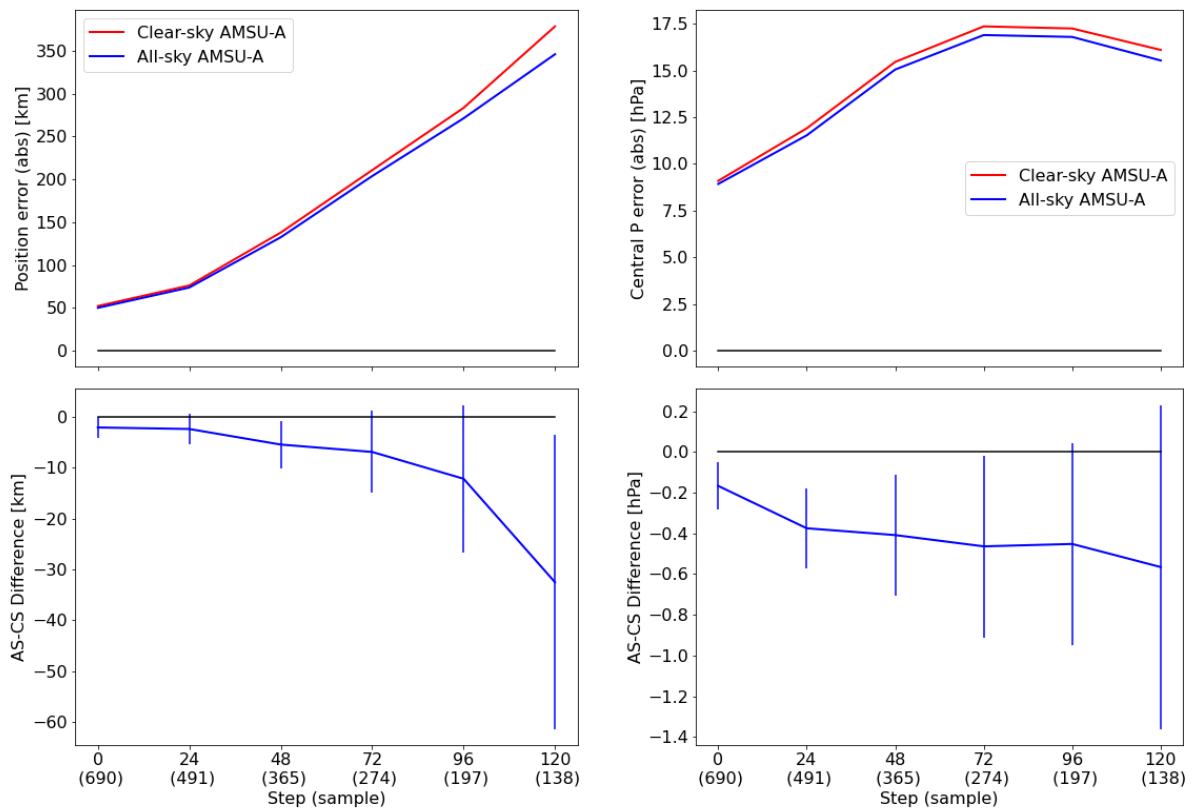
Figure 11: Tropical cyclone verification for July through November 2019, comparing track position (left) and central pressure (right) errors from all-sky and clear-sky AMSU-A. Only cyclones that appear in the tracker for both experiments are included in the statistics. Vertical bars represent estimates of 95% confidence intervals, calculated as $1.96\sigma/\sqrt{n}$; these do not account for potentially correlated verification errors, such as those from successive forecasts of the same cyclone.
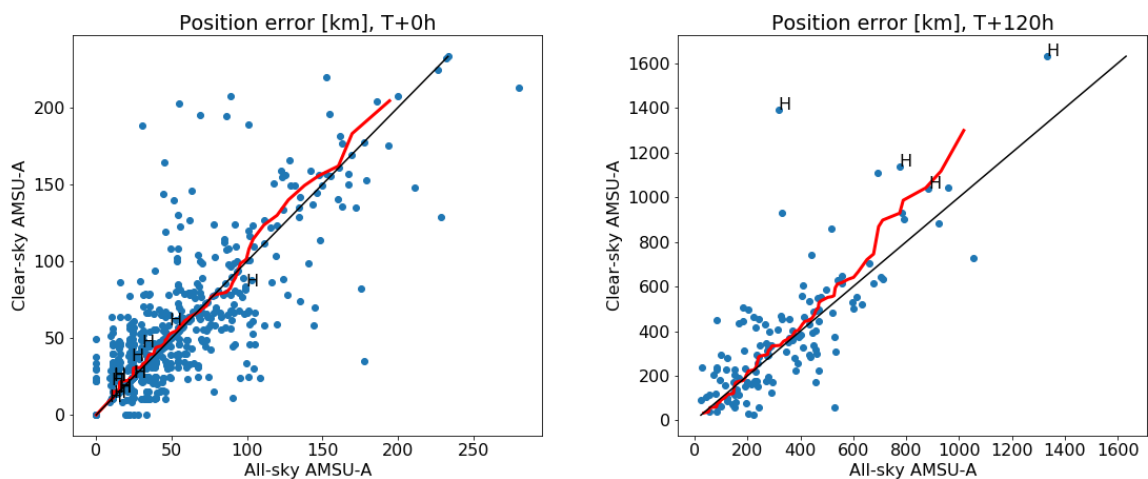

Figure 12: As in Fig. 11, but scatter plots of position error at analysis time (D+0) and 120 hours (D+5). Points indicating Humberto are marked with a 'H' on the plot.

for the present findings. In the following, we will further examine the performance of all-sky AMSU-A assimilation for selected cyclone cases.

3.3.2 Humberto

In mid September 2019, Hurricane Humberto reached an intensity of category 3 on the Saffir-Simpson scale and appeared to threaten the east coast of the United States. Its track then took a sharp turn to the east, ultimately moving past Bermuda and into the north Atlantic. Uncertainties in the track and eventual extratropical transition of Humberto led to a multi-day drop in forecast skill over Europe a week later, just two weeks after a similar effect was witnessed from Hurricane Dorian[2].

The most striking aspect of all-sky assimilation near tropical cyclones is that it fills a large gap in data usage left by clear-sky assimilation. Figure 13 displays such a hole caused by cloud screening, compared to the more even spatial distribution of all-sky observations assimilated. A second potentially important aspect is, in some areas, the predominance of negative departures in the clear-sky approach. For example, broad areas of negative departures are seen nearly encircling the islands of Cuba and Hispaniola to the north and east, and including the immediate region of Humberto. The additional all-sky observations in these areas tend to bring more positive departures. This may back up one of the key motivations for doing all-sky assimilation: to achieve a more balanced distribution of departures (Bauer *et al.*, 2010; Geer *et al.*, 2012). A more balanced distribution of increments in areas of low-level water cloud was also one of the main benefits of all-sky assimilation observed by Zhu *et al.* (2016).

In addition to observations near the cyclone itself, Fig. 13 also shows that downstream observations hundreds of kilometres away are also now used in all-sky, in this case filling a gap for MW temperature sounding that existed in the north Atlantic, southeast of Newfoundland. These areas are both potentially significant, as all-sky assimilation near the cyclone itself may improve the analysis of cyclone location, pressure, and winds, whereas changes to the steering flow from the synoptic analysis could affect the cyclone's eventual track several days later (e.g. McNally *et al.*, 2014). The other salient feature of Fig. 13 is the thinning difference between all-sky and clear-sky data streams, described in Section 2.1.

To visualise the effect of using observations nearby and downstream of a tropical cyclone, Figure 14 shows FSOI values from channel 5 on four consecutive days along the track of Hurricane Humberto. Only the largest (positive and negative) values are plotted, emphasising observations with a significant effect on the forecast. In other words, there is no pre-selection for observations near the cyclone track— these points appear near the track because that is where FSOI values for AMSU-A radiances are largest. It is clear that all-sky temperature sounding does not have much effect on September 15th, but on the 16th after making a sharp turn away from land there are several channel 5 observations that aided the forecast. Moving further ahead, the impactful observations are more spread out, albeit still mostly in the direction of the eventual track. Similar figures were produced for the clear-sky assimilation, showing no such large absolute FSOI values for channel 5, and most of the observations near the core were removed (not shown). It is worth noting that FSOI suggests that some of the observations used in all-sky had a large detrimental effect on the forecast (i.e. positive FSOI), especially on the 17th. The interpretation of this is not clear, though we note that large positive FSOI values occasionally also occur for the clear-sky assimilation.

This sequence shows that all-sky temperature sounding was consequential in shaping the short-range forecast of Hurricane Humberto, first by informing the forecast with observations of the cyclone itself

---

[2]https://www.ecmwf.int/sites/default/files/elibrary/2020/19546-annual-report-2019.pdf
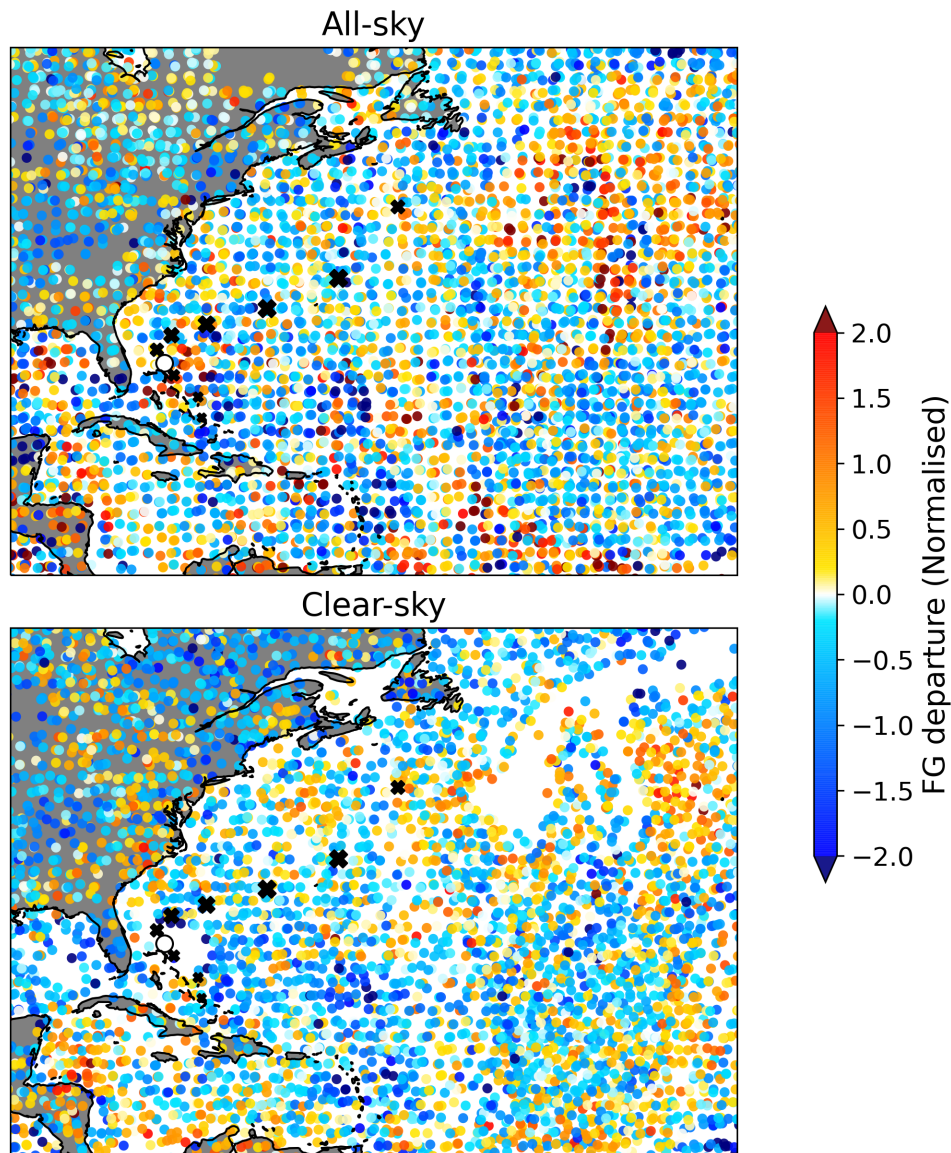
Figure 13: First guess departures for all-sky (top) and clear-sky (bottom) channel 5 observations assimilated during the 0Z long window on September 15, 2019, normalised by the observation errors assigned. The National Hurricane Center (NHC) best track locations at 0Z over the life of Humberto are given by a black X, with a white circle showing the hurricane location on this date, just east of Florida. Data from all AMSU-A sensors are shown together. Departures are normalised by the assigned observation errors.

as it moved into the north Atlantic, and then downstream as it began extratropical transition. In the experimentation, the all-sky results showed a mitigated forecast bust over Europe at day 6-8 in the period Sept. 22-24; this was one of the worst forecast busts for Europe that season, a result consistent between the lower resolution experiment and the high-resolution forecast in ECMWF operations. Although it is a logical leap to conclude that a few AMSU-A observations near Humberto were indeed the cause for mitigating a downstream forecast bust, this analysis shows that many previously unused AMSU-A observations were influential near the cyclone itself and also downstream as the cyclone sped up and moved toward Europe.
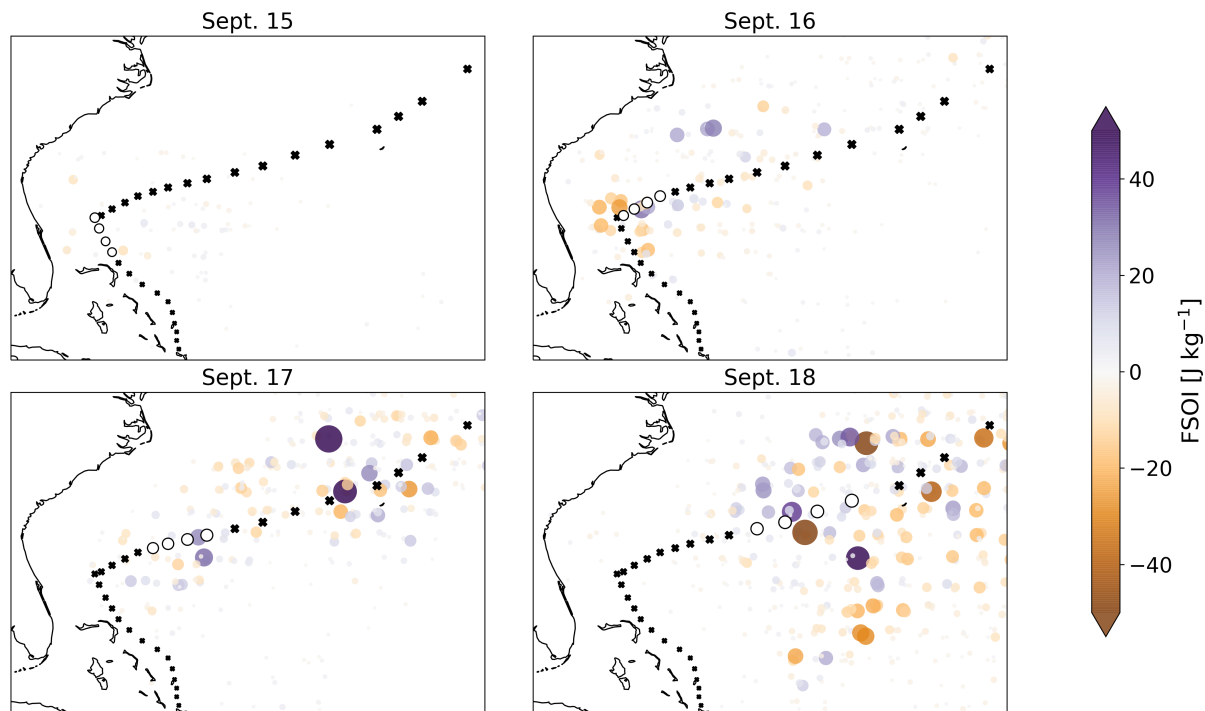
Figure 14: FSOI values for AMSU-A channel 5 along the track of Hurricane Humberto, spanning 15th to 18th September, 2019. Only observations with abs(FSOI) > 1.0 are shown, and the dot size is also a function of abs(FSOI) to emphasise impactful observations. As in Fig. 13, the cyclone track and positions on each date are given for every 6 hours.

3.3.3 Jerry

As seen in Figure 10, a bright spot exists in the all-sky FSOI map east of Florida and north of Puerto Rico. Upon closer investigation, this large FSOI signal results from a single assimilation window alone, 0Z on 23rd September. This was solely from observations near Hurricane Jerry, a tropical cyclone that peaked as a Category 2 hurricane on the 20th and had decayed to tropical storm strength[3]. This was a period in which synoptic-scale wind shear played a critical role, causing the cyclone to substantially weaken rather than re-intensify, as some forecast models had suggested[4].

The case of Hurricane Jerry is noteworthy for how distributed this signal is amongst channels and satellite platforms, despite being concentrated in a small region. Six satellite platforms contributed single observations with FSOI magnitudes greater than $-100 \, \mathrm{J \, kg^{-1}}$; of these, most were from channel 5, though there were also several channel 6 and 7 observations with very large FSOI. A majority of these very high-impact observations were from NOAA-15 and NOAA-18, particularly the very low-noise channel 5 on NOAA-15 and channel 6 on NOAA-18. This case underscores the value of ageing platforms and the benefits of having several satellites with sounding capabilities working in concert (Duncan *et al.*, In press).

Figure 15 shows the analysis increments from all-sky and clear-sky assimilation around Hurricane Jerry. For this comparison, the clear-sky assimilation was begun from the same initial state as the all-sky exper-

---

[3] https://www.nhc.noaa.gov/data/tcr/AL102019_Jerry.pdf
[4] https://www.ecmwf.int/en/forecasts/charts/tcyclone/tc_plumes?facets=undefined& time=2019092300,0,2019092300&unique_id=10L_JERRY_2019
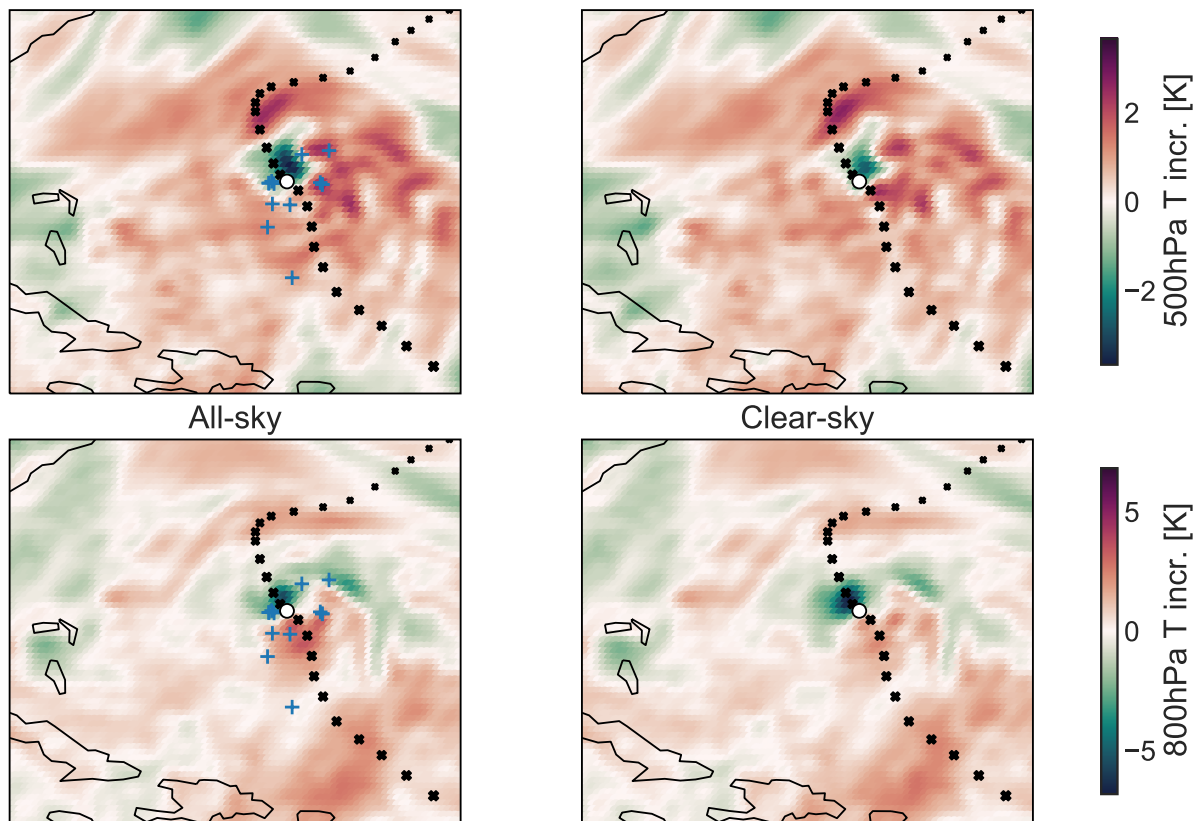
Figure 15: Analysis increments for temperature at 500hPa (top) and 800hPa (bottom), 23rd September 2019 at 0Z, for all-sky (left) and clear-sky (right) assimilation of AMSU-A. Both started from the same initial state. Tropical storm Jerry and its track are given. All-sky AMSU-A observations with FSOI magnitudes larger than $-100\,\mathrm{J\,kg^{-1}}$ are shown as purple crosses.

iment so as to better compare the increment maps. The most impactful all-sky observations (also shown in the figure) are within a few hundred kilometres of the cyclone's centre and appear to cause tighter gradients and greater structure in the temperature analysis at mid-levels. Through 4D-Var these signals affect the whole circulation, and significant differences are noticeable in the increments down to the surface. The modified increment changes near the cyclone core give a possible mechanism for the minor improvements in intensity noted earlier for the whole season (Fig. 11). While by no means representative of all-sky temperature assimilation in tropical cyclones, this case indicates that it is possible to witness a considerable effect from all-sky temperature observations within the cyclone circulation itself, rather than just impacting the steering flow.

4   Conclusions

Successful all-sky assimilation of microwave temperature sounder radiances at ECMWF is the result of incremental progress in various aspects of data assimilation and radiative transfer modelling. Viewed in the context of overall microwave assimilation at ECMWF, 50 GHz temperature sounding channels are now used in conjunction with an extensive set of imager and humidity sounding channels in all-sky conditions, spanning 18 to 190 GHz. The upgrade to IFS Cycle 47R3 will cause the number of all-sky sensors to increase by about half in autumn 2021. This represents a powerful and unified constraint for

atmospheric temperature and humidity as well as clouds and precipitation.

Methodologically, the following aspects were crucial for enabling the move from clear-sky to all-sky assimilation of AMSU-A:

- The distribution of radiances after thinning imitates that of clear-sky (at least, before the cloud screening) both regionally and as a function of scan position

- The use of a well-tuned observation error model that depends on the meteorological situation

- A larger VarQC a priori probability of gross error is balanced with slightly reduced observation error in clear-sky conditions; this helps retain impact in clear skies whilst minimising the impact of outliers elsewhere

- Advances in scattering radiative transfer in recent years have permitted assimilation even in deep convective clouds, which increases the number of additional observations that can be provided by all-sky assimilation

The eventual all-sky configuration for AMSU-A blends elements of the previous clear-sky treatment of temperature sounders with those of all-sky humidity sounders, now permitting useful information to be extracted from AMSU-A radiances in areas of cloud and precipitation, from stratocumulus regions to tropical cyclones. As a consequence, this increases the total number of radiances assimilated, most substantially in the mid-latitude storm tracks.

All-sky assimilation has herein been shown to replicate and exceed the forecast impact of the previous clear-sky usage of AMSU-A, as judged by medium-range forecast scores and verification against independent observations. Some highlights of the results presented include:

- Greater and more balanced sampling, especially for high-impact weather; the number of assimilated radiances from channels 5 and 6 increase by 13% and 6%, respectively

- Z500 RMSE improves by about 0.5% up through at least day 2 in both hemispheres

- Short-range forecasts of humidity improve, as seen in better fits to infrared, microwave, and conventional observations

Despite using channels primarily sensitive to the mid troposphere and above, the effects of all-sky AMSU-A assimilation are felt throughout the troposphere, including visible improvements to surface pressure and near-surface winds over ocean. And while only one season was examined, there are encouraging signs that all-sky temperature sounding can aid in tropical cyclone forecasting by adding information in data-sparse regions at mid-levels, near the cyclone core and also downstream, potentially helping to mitigate errors that occur during the extratropical transition of cyclones.

The methodology developed here for AMSU-A is expected to be applicable to a range of similar MW sounders with channels in the 50 GHz band. In the near-term, we expect to adapt the all-sky approach to the ATMS sensor, which is now the only MW instrument still assimilated in clear-sky in the ECMWF system. Furthermore, the first MWTS-3 (MicroWave Temperature Sounder-3) instrument has recently been launched on the Chinese FY-3E satellite, with a channel complement comparable to AMSU-A. Future sensors include the MicroWave Sounder (MWS) on Metop-SG and the MW sounding instrument on the Arctic Weather Satellite (AWS).

There remain ways to further optimise the total information content exploited from AMSU-A. Currently the assimilation of AMSU-A is restricted to channels 5-14. With the move to all-sky assimilation, it is attractive to extend this to other channels with stronger cloud signals that were excluded from the clear-sky assimilation. Experimentation that includes active use of channel 4, for instance, shows some promise. Further, the lower frequency channels at 23.8 and 31.4 GHz could be considered for active assimilation; such channels are already successfully assimilated from conically scanning MW imagers in the ECMWF system, and they are included in the operational assimilation of cloud-affected radiances elsewhere (Zhu *et al.*, 2016). Other possible advances include increased data usage over complex terrain or snow- and sea-ice covered surfaces, and treating correlated errors in precipitation. Moving AMSU-A to all-sky conditions is a significant step towards the ultimate goal of assimilating all microwave radiances over all surfaces and in all atmospheric conditions.

Acknowledgements

References

Andersson, E. and Järvinen, H. (1999). Variational quality control. *Quart. J. Roy. Meteor. Soc.*, **125**(554), 697–722, doi:10.1002/qj.49712555416, URL https://rmets.onlinelibrary.wiley.com/doi/abs/10.1002/qj.49712555416.

Andersson, E., Pailleux, J., Thépaut, J.-N., Eyre, J. R., McNally, A. P., Kelly, G. A. and Courtier, P. (1994). Use of cloud-cleared radiances in three/four-dimensional variational data assimilation. *Quart. J. Roy. Meteor. Soc.*, **120**(517), 627–653, doi:10.1002/qj.49712051707, URL https://rmets.onlinelibrary.wiley.com/doi/abs/10.1002/qj.49712051707.

Baordo, F. and Geer, A. J. (2016). Assimilation of SSMIS humidity-sounding channels in all-sky conditions over land using a dynamic emissivity retrieval. *Quart. J. Roy. Meteor. Soc.*, **142**(700), 2854–2866, doi:10.1002/qj.2873, URL https://rmets.onlinelibrary.wiley.com/doi/abs/10.1002/qj.2873.

Bauer, P., Geer, A. J., Lopez, P. and Salmond, D. (2010). Direct 4D-Var assimilation of all-sky radiances. Part I: Implementation. *Quart. J. Roy. Meteor. Soc.*, **136**(652), 1868–1885, doi:10.1002/qj.659, URL https://rmets.onlinelibrary.wiley.com/doi/abs/10.1002/qj.659.

Bauer, P., Moreau, E., Chevallier, F. and O'Keeffe, U. (2006). Multiple-scattering microwave radiative transfer for data assimilation applications. *Quart. J. Roy. Meteor. Soc.*, **132**(617), 1259–1281, doi:10.1256/qj.05.153, URL https://rmets.onlinelibrary.wiley.com/doi/abs/10.1256/qj.05.153.

Bauer, P. and Mugnai, A. (2003). Precipitation profile retrievals using temperature-sounding microwave observations. *J. Geophys. Res. Atmos.*, **108**(D23), doi:10.1029/2003JD003572, URL https://agupubs.onlinelibrary.wiley.com/doi/abs/10.1029/2003JD003572.

Bell, W., English, S. J., Candy, B., Atkinson, N., Hilton, F., Baker, N., Swadley, S. D., Campbell, W. F., Bormann, N., Kelly, G. and Kazumori, M. (2008). The assimilation of SSMIS radiances in numerical weather prediction models. *IEEE T. Geosci. Remote Sens.*, **46**(4), 884–900, doi:10.1109/TGRS.2008.917335, URL https://ieeexplore.ieee.org/abstract/document/4468717.

Bormann, N. (2017). Slant path radiative transfer for the assimilation of sounder radiances. *Tellus A*, **69**(1), 1272779, doi:10.1080/16000870.2016.1272779, URL https://doi.org/10.1080/16000870.2016.1272779.

Bormann, N., Lawrence, H. and Farnan, J. (2019). Global observing system experiments in the ECMWF assimilation system. *Technical Report 839*, ECMWF Tech. Memo., doi:10.21957/sr184iyz, URL https://www.ecmwf.int/node/18859.

Bormann, N., Lupu, C., Geer, A. J., Lawrence, H., Weston, P. and English, S. (2017). Assessment of the forecast impact of surface-sensitive microwave radiances over land and sea-ice. *Technical Report 804*, ECMWF Tech. Memo., doi:10.21957/qyh34roht, URL https://www.ecmwf.int/node/17674.

Boukabara, S.-A., Jones, E., Geer, A., Kazumori, M., Garrett, K. and Maddy, E. (2020). Assimilation of precipitation observations from space into numerical weather prediction (NWP). In V. Levizzani, C. Kidd, D. B. Kirschbaum, C. D. Kummerow, K. Nakamura and F. J. Turk (Eds), *Satellite Precipitation Measurement*, Vol. 2, chapter 48, pp. 941–982, Springer Nature, ISBN 978-3-030-35798-6, doi:10.1007/978-3-030-35798-6_24, URL https://doi.org/10.1007/978-3-030-35798-6_24.

Brueske, K. F. and Velden, C. S. (2003). Satellite-based tropical cyclone intensity estimation using the NOAA-KLM series Advanced Microwave Sounding Unit (AMSU). *Mon. Weather Rev.*, **131**(4), 687 – 697, doi:10.1175/1520-0493(2003)131⟨0687:SBTCIE⟩2.0.CO;2, URL https://journals.ametsoc.org/view/journals/mwre/131/4/1520-0493_2003_131_0687_sbtcie_2.0.co_2.xml.

Cardinali, C. (2009). Monitoring the observation impact on the short-range forecast. *Quart. J. Roy. Meteor. Soc.*, **135**(638), 239–250, doi:10.1002/qj.366, URL https://rmets.onlinelibrary.wiley.com/doi/abs/10.1002/qj.366.

Duncan, D. I., Bormann, N. and Hólm, E. (In press). On the addition of microwave sounders and numerical weather prediction skill. *Quart. J. Roy. Meteor. Soc.*, doi:10.1002/qj.4149, URL https://doi.org/10.1002/qj.4149.

Durden, S. L. (2013). Observed tropical cyclone eye thermal anomaly profiles extending above 300 hPa. *Mon. Weather Rev.*, **141**(12), 4256 – 4268, doi:10.1175/MWR-D-13-00021.1, URL https://journals.ametsoc.org/view/journals/mwre/141/12/mwr-d-13-00021.1.xml.

ECMWF (2020). *IFS Documentation CY47R1, Part II: Data Assimilation*. ECMWF, doi:10.21957/0gtybbwp9, URL https://www.ecmwf.int/node/19746.

English, S., McNally, T., Bormann, N., Isaksen, L., Lupu, C., Ingleby, B. and Dahoui, M. (2020). Guidance for interpretation of OSE and FSOI to support WIGOS design and assessment. *Technical Report RD20-134*, ECMWF RD Memo., Shinfield Park, Reading.

English, S. J., Renshaw, R. J., Dibben, P. C., Smith, A. J., Rayer, P. J., Poulsen, C., Saunders, F. W. and Eyre, J. R. (2000). A comparison of the impact of TOVS and ATOVS satellite sounding data on the accuracy of numerical weather forecasts. *Quart. J. Roy. Meteor. Soc.*, **126**(569), 2911–2931, doi:10.1002/qj.49712656915, URL https://rmets.onlinelibrary.wiley.com/doi/abs/10.1002/qj.49712656915.

Errico, R. M., Bauer, P. and Mahfouf, J.-F. (2007). Issues regarding the assimilation of cloud and precipitation data. *J. Atmos. Sci.*, **64**, 3785 – 3798, doi:10.1175/2006JAS2044.1, URL https://doi.org/10.1175/2006JAS2044.1.

Geer, A. J. (2016). Significance of changes in medium-range forecast scores. *Tellus A*, **68**(1), 30229, doi:10.3402/tellusa.v68.30229, URL https://doi.org/10.3402/tellusa.v68.30229.

Geer, A. J. and Baordo, F. (2014). Improved scattering radiative transfer for frozen hydrometeors at microwave frequencies. *Atmos. Meas. Tech.*, **7**(6), 1839–1860, doi:10.5194/amtd-7-1749-2014, URL https://amt.copernicus.org/articles/7/1839/2014/.

Geer, A. J., Baordo, F., Bormann, N., Chambon, P., English, S. J., Kazumori, M., Lawrence, H., Lean, P., Lonitz, K. and Lupu, C. (2017). The growing impact of satellite observations sensitive to humidity, cloud and precipitation. *Quart. J. Roy. Meteor. Soc.*, **143**(709), 3189–3206, doi:10.1002/qj.3172, URL https://rmets.onlinelibrary.wiley.com/doi/abs/10.1002/qj.3172.

Geer, A. J., Baordo, F., Bormann, N. and English, S. (2014). All-sky assimilation of microwave humidity sounders. *Technical Report 741*, ECMWF Tech. Memo., doi:10.21957/obosmx154, URL https://www.ecmwf.int/node/9507.

Geer, A. J. and Bauer, P. (2010). Enhanced use of all-sky microwave observations sensitive to water vapour, cloud and precipitation. *Technical Report 20*, EUMETSAT/ECMWF Fellowship Programme Research Report, URL https://www.ecmwf.int/node/9506, also published as ECMWF Technical Memorandum No.620.

Geer, A. J. and Bauer, P. (2011). Observation errors in all-sky data assimilation. *Quart. J. Roy. Meteor. Soc.*, **137**(661), 2024–2037, doi:10.1002/qj.830, URL https://rmets.onlinelibrary.wiley.com/doi/abs/10.1002/qj.830.

Geer, A. J., Bauer, P. and English, S. (2012). Assimilating AMSU-A temperature sounding channels in the presence of cloud and precipitation. *Technical Report 24*, EUMETSAT/ECMWF Fellowship Programme Research Report, URL https://www.ecmwf.int/node/9513, also published as ECMWF Technical Memorandum 670.

Geer, A. J., Bauer, P. and O'Dell, C. W. (2009). A revised cloud overlap scheme for fast microwave radiative transfer in rain and cloud. *J. Appl. Meteorol. and Climatol.*, doi: 10.1175/2009JAMC2170.1, URL https://journals.ametsoc.org/view/journals/apme/48/11/2009jamc2170.1.xml.

Geer, A. J., Lonitz, K., Weston, P., Kazumori, M., Okamoto, K., Zhu, Y., Liu, E. H., Collard, A., Bell, W., Migliorini, S., Chambon, P., Fourrié, N., Kim, M.-J., Köpken-Watts, C. and Schraff, C. (2018). All-sky satellite data assimilation at operational weather forecasting centres. *Quart. J. Roy. Meteor. Soc.*, **144**(713), 1191–1217, doi:10.1002/qj.3202, URL https://rmets.onlinelibrary.wiley.com/doi/abs/10.1002/qj.3202.

Grody, N., Zhao, J., Ferraro, R., Weng, F. and Boers, R. (2001). Determination of precipitable water and cloud liquid water over oceans from the NOAA 15 advanced microwave sounding unit. *J. Geophys. Res. Atmos.*, **106**(D3), 2943–2953, doi:10.1029/2000JD900616, URL https://agupubs.onlinelibrary.wiley.com/doi/abs/10.1029/2000JD900616.

Han, W. and Bormann, N. (2016). Constrained adaptive bias correction for satellite radiance assimilation in the ECMWF 4D-Var system. *Technical Report 783*, ECMWF Tech. Memo., doi: 10.21957/rex0omex, URL https://www.ecmwf.int/node/16712.

Karbou, F., Gérard, E. and Rabier, F. (2006). Microwave land emissivity and skin temperature for AMSU-A and -B assimilation over land. *Quart. J. Roy. Meteor. Soc.*, **132**(620), 2333–2355, doi:10.1256/qj.05.216, URL https://rmets.onlinelibrary.wiley.com/doi/abs/10.1256/qj.05.216.

Kazumori, M. and English, S. J. (2015). Use of the ocean surface wind direction signal in microwave radiance assimilation. *Quart. J. Roy. Meteor. Soc.*, **141**(689), 1354–1375, doi:10.1002/qj.2445, URL https://rmets.onlinelibrary.wiley.com/doi/abs/10.1002/qj.2445.

Knaff, J. A., Seseske, S. A., DeMaria, M. and Demuth, J. L. (2004). On the influences of vertical wind shear on symmetric tropical cyclone structure derived from AMSU. *Mon. Weather Rev.*, **132**(10), 2503 – 2510, doi:10.1175/1520-0493(2004)132⟨2503:OTIOVW⟩2.0.CO;2, URL https://journals.ametsoc.org/view/journals/mwre/132/10/1520-0493_2004_132_2503_otiovw_2.0.co_2.xml.

Knapp, K. R., Kruk, M. C., Levinson, D. H., Diamond, H. J. and Neumann, C. J. (2010). The international best track archive for climate stewardship (IBTrACS): Unifying tropical cyclone data. *Bull. Amer. Meteor. Soc.*, **91**(3), 363 – 376, doi:10.1175/2009BAMS2755.1, URL https://journals.ametsoc.org/view/journals/bams/91/3/2009bams2755_1.xml.

Lawrence, H., Bormann, N. and English, S. (2015). Scene-dependent observation errors for the assimilation of AMSU-A. *Technical Report 39*, EUMETSAT/ECMWF Fellowship Programme Research Report, Shinfield Park, Reading, URL https://www.ecmwf.int/node/10669.

Lawrence, H., Bormann, N., Geer, A. J., Lu, Q. and English, S. J. (2018). Evaluation and assimilation of the microwave sounder MWHS-2 onboard FY-3C in the ECMWF numerical weather prediction system. *IEEE T. Geosci. Remote Sens.*, **56**(6), 3333–3349, doi:10.1109/TGRS.2018.2798292, URL https://doi.org/10.1109/TGRS.2018.2798292.

Magnusson, L. (2017). Diagnostic methods for understanding the origin of forecast errors. *Quart. J. Roy. Meteor. Soc.*, **143**(706), 2129–2142, doi:10.1002/qj.3072, URL https://rmets.onlinelibrary.wiley.com/doi/abs/10.1002/qj.3072.

Massart, S., Bormann, N., Bonavita, M. and Lupu, C. (2021). Multi-sensor analyses of the skin temperature for the assimilation of satellite radiances in the European Centre for Medium-Range Weather Forecasts (ECMWF) Integrated Forecasting System (IFS, cycle 47R1). *Geosci. Model Dev.*, **14**(9), 5467–5485, doi:10.5194/gmd-14-5467-2021, URL https://gmd.copernicus.org/articles/14/5467/2021/.

McNally, T., Bonavita, M. and Thépaut, J.-N. (2014). The role of satellite data in the forecasting of Hurricane Sandy. *Mon. Weather Rev.*, **142**(2), 634–646, doi:10.1175/MWR-D-13-00170.1, URL https://doi.org/10.1175/MWR-D-13-00170.1.

Migliorini, S. and Candy, B. (2019). All-sky satellite data assimilation of microwave temperature sounding channels at the Met Office. *Quart. J. Roy. Meteor. Soc.*, **145**(719), 867–883, doi:10.1002/qj.3470, URL https://rmets.onlinelibrary.wiley.com/doi/abs/10.1002/qj.3470.

Munchak, S. J. and Skofronick-Jackson, G. (2013). Evaluation of precipitation detection over various surfaces from passive microwave imagers and sounders. *Atmos. Res.*, **131**, 81 – 94, doi:10.1016/j.atmosres.2012.10.011, URL http://www.sciencedirect.com/science/article/pii/S0169809512003377.

Peubey, C. and McNally, A. (2009). Characterization of the impact of geostationary clear-sky radiances on wind analyses in a 4D-Var context. *Quart. J. Roy. Meteor. Soc.*, **135**(644), 1863–1876, doi:10.1002/qj.500, URL https://rmets.onlinelibrary.wiley.com/doi/abs/10.1002/qj.500.

Saunders, R., Hocking, J., Turner, E., Rayer, P., Rundle, D., Brunel, P., Vidot, J., Roquet, P., Matricardi, M., Geer, A., Bormann, N. and Lupu, C. (2018). An update on the RTTOV fast radiative transfer model (currently at version 12). *Geosci. Model Dev.*, **11**(7), 2717–2737, doi:10.5194/gmd-11-2717-2018, URL https://gmd.copernicus.org/articles/11/2717/2018/.

Tian, X. and Zou, X. (2016). ATMS- and AMSU-A-derived hurricane warm core structures using a modified retrieval algorithm. *J. Geophys. Res. Atmos.*, **121**(21), 12,630–12,646, doi:10.1002/2016JD025042, URL https://agupubs.onlinelibrary.wiley.com/doi/abs/10.1002/2016JD025042.

Tong, M., Zhu, Y., Zhou, L., Liu, E., Chen, M., Liu, Q. and Lin, S.-J. (2020). Multiple hydrometeors all-sky microwave radiance assimilation in FV3GFS. *Mon. Weather Rev.*, **148**(7), 2971–2995, doi:10.1175/MWR-D-19-0231.1, URL https://doi.org/10.1175/MWR-D-19-0231.1.

van der Grijn, G. (2002). Tropical cyclone forecasting at ECMWF: new products and validation. *Technical Report 386*, ECMWF Tech. Memo., Shinfield Park, Reading, doi:10.21957/c8525o38f, URL https://www.ecmwf.int/node/13266.

Weston, P., Geer, A. J. and Bormann, N. (2019). Investigations into the assimilation of AMSU-A in the presence of cloud and precipitation. *Technical Report 50*, EUMETSAT/ECMWF Fellowship Programme Research Report, doi:10.21957/ewahn9ce, URL https://www.ecmwf.int/node/19221.

Zhu, T. and Weng, F. (2013). Hurricane Sandy warm-core structure observed from Advanced Technology Microwave Sounder. *Geophys. Res. Lett.*, **40**(12), 3325–3330, doi:10.1002/grl.50626, URL https://agupubs.onlinelibrary.wiley.com/doi/abs/10.1002/grl.50626.

Zhu, Y., Gayno, G., Purser, R. J., Su, X. and Yang, R. (2019). Expansion of the all-sky radiance assimilation to ATMS at NCEP. *Mon. Weather Rev.*, **147**(7), 2603–2620, doi:10.1175/MWR-D-18-0228.1, URL https://doi.org/10.1175/MWR-D-18-0228.1.

Zhu, Y., Liu, E., Mahajan, R., Thomas, C., Groff, D., Delst, P. V., Collard, A., Kleist, D., Treadon, R. and Derber, J. C. (2016). All-sky microwave radiance assimilation in NCEP's GSI analysis system. *Mon. Weather Rev.*, **144**(12), 4709 – 4735, doi:10.1175/MWR-D-15-0445.1, URL https://journals.ametsoc.org/view/journals/mwre/144/12/mwr-d-15-0445.1.xml.